4232 *Inorg. Chem.* **2010**, *49*, 4232–4244
DOI: 10.1021/ic100072a

Inorganic Chemistry
Article

Rhomboidal Heterometallic Alkynyl Based Pt_2Cd_2 Clusters: Structural, Photophysical, and Theoretical Studies

Jesús R. Berenguer, Julio Fernández, Belén Gil, Elena Lalinde,* and Sergio Sánchez

Departamento de Química-Grupo de Síntesis Química de La Rioja, UA-CSIC, Universidad de La Rioja, 26006, Logroño, Spain

Received January 13, 2010

Reactions between $[Pt(C{\equiv}CR)_4]^{2-}$ (R=Tol **a**, C_6H_4OMe-4 **b**, C_6H_4OMe-3 **c**) and Cd^{2+} depend on the media and the alkynyl substituent, leading to the formation of yellow tetranuclear solvate complexes $[Pt(C{\equiv}CR)_4Cd(acetone)]_2$ **1a**, **b**$(acetone)_2$ and $[Pt(C{\equiv}CC_6H_4OMe\text{-}3)_4Cd(dmso)]_2$ **1c**$(\mathbf{dmso})_\mathbf{2}$ or white polymeric solvate-free species $[Pt(C{\equiv}CR)_4Cd]_x$ **1′a**−**c**. Treatment of **1a,b**$(acetone)_2$ or **1′a**−**c** with N-donor ligands affords a series of tetranuclear clusters $[Pt(C{\equiv}CR)_4CdL]_2$ (L=py; **2a**−**c**. R=Tol; L=$NC_5H_4CH_3$-4 **3**, $NC_5H_4CF_3$-4 **4**, pzH **5**). X-ray crystallographic studies reveal that, in the tolyl complexes (**2a**, **4**, and **5**), the Cd-L^{2+} unit is closely bonded to one Pt−C_α(acetylide) bond (Pt−Cd = 2.7, Cd−C_α ∼ 2.48 Å), and the resulting "$Pt(C{\equiv}CTol)_4CdL$" unit dimerizes by two additional η^2-Cd-acetylide and a weaker Pt···Cd bonding interaction leading to a planar unsymmetrical rhomboidal metal core. By contrast, the *m*-methoxyphenyl derivatives (**2c**, **1c**$(\mathbf{dmso})_\mathbf{2}$) form symmetrical Pt_2Cd_2 cores, with each Cd bonded (coordination number, C.N.=5) to the incoming ligand (pyridine **2c**, dmso **1c**$(\mathbf{dmso})_\mathbf{2}$) and four Pt−$C_\alpha$ bonds (Pt−Cd 2.85; Cd−C_α 2.470(10)−2.551(5) Å) of different Pt^{II} fragments. Evidence of ligand dissociation was found for the solvate (**1a,b**$(\mathbf{acetone})_\mathbf{2}$, **1c**$(\mathbf{dmso})_\mathbf{2}$) and $NC_5H_4CF_3$-4 (**4**) derivatives by NMR and UV−vis absorption spectra. All tetranuclear aggregates exhibit bright blue to green luminescence in the solid state. Time-dependent density functional theory (TD-DFT) calculations were performed to shed light on the nature of the electronic transitions. In the solvate **1a,b**$(\mathbf{acetone})_\mathbf{2}$ and **1c**$(\mathbf{dmso})_\mathbf{2}$, emissions have been assigned to a platinum-alkynyl to cadmium charge transfer (^{3}MLM′CT), mixed with some intraligand ^{3}IL(C≡CR) character. In the imine derivatives **2**−**5**, they are suggested to come from an excited state of large Pt(d)/πC≡CR→π^*(imine) MLL′CT character, mixed with some Pt(d)/π(C≡CR)→Pt_2Cd_2/π^*C≡CR (ML′M′CT) contribution.

Introduction

Transition metal complexes with alkynyl ligands have been widely used in the design of photoluminescent materials with interesting spectroscopic properties[1−10] suitable in the field of fundamental and applied material science.[11] In these systems excited-state properties are controlled by changing the metal, the coligands, or the electronic nature of the alkynyl fragments.

Recently, homo and heteropolynuclear aggregates containing closed or pseudo closed shell (d^{10}, d^8, $d^{10}s^2$) metal ions have also gained increasing interest, in part because of their intriguing luminescent properties, which have been attributed to the presence of metallophilic bonds.[12] In this respect, considerable experimental work has clearly demonstrated the influence of the metallophilic interactions in the structure and luminescence of alkynyl metal complexes of Cu^I, Ag^I, Au^I, Hg^{II} (d^{10})[1,3−6] and Pt^{II}(d^8).[6,13,14] Despite the fact that the chemistry of *heteropolynuclear* complexes with alkynyl bridging ligands has been an active research area, studies relative to their optical properties are scarce in the literature.[4,8,15−17] Within this field we and others have demonstrated that homoleptic[18−28] and heteroleptic[29−36] anionic σ-alkynyl platinates are excellent building blocks for the synthesis of heteropolynuclear Pt−M (M = d^{10}, s^2) complexes that show interesting structures and intriguing photophysical properties. These investigations have allowed us to observe that, depending on the Lewis-acidic metal and the basic platinate

*To whom correspondence should be addressed. E-mail: elena.lalinde@unirioja.es.

(1) Wong, W.-Y. *Coord. Chem. Rev.* **2007**, *251*, 2400.
(2) Hissler, M.; McGarrah, J. E.; Connick, W. B.; Geiger, D. K.; Cummings, S. D.; Eisenberg, R. *Coord. Chem. Rev.* **2000**, *208*, 115.
(3) Yam, V. W.-W.; Lo, K. K.-W. *Chem. Soc. Rev.* **1999**, *28*, 323.
(4) Yam, V. W.-W.; Lo, K. K.-W.; Wong, K. M.-C. *J. Organomet. Chem.* **1999**, *578*, 3.
(5) Yam, V. W.-W.; Lo, W.-Y.; Lam, C.-H.; Fung, W. K.-M.; Wong, K. M.-C.; Lau, V. C.-Y.; Zhu, N. *Coord. Chem. Rev.* **2003**, *245*, 39.
(6) Yam, V. W.-W. *J. Organomet. Chem.* **2004**, *689*, 1393.
(7) Wong, W.-Y. *Dalton Trans.* **2007**, 4495.
(8) Chen, Z.-N.; Zhao, N.; Fan, Y.; Ni, J. *Coord. Chem. Rev.* **2009**, *253*, 1.
(9) Castellano, F. N.; Pomestchenko, I. E.; Shikhova, E.; Hua, F.; Muro, M. L.; Rajapakse, N. *Coord. Chem. Rev.* **2006**, *250*, 1819.
(10) Ziessel, R.; Hissler, M.; El-ghayoury, A.; Harriman, A. *Coord. Chem. Rev.* **1998**, *178*−*180*, 1251.

 Published on Web 04/09/2010

substrate, the final heterometallic aggregates are basically stabilized: (a) by η^2-alkynyl−M bonds and Pt···M secondary interactions or (b) by significant Pt−M bonds and/or secondary η(alkyne)···M bonds. In this respect, while coinage d^{10} metal ions such as Cu^I or Ag^I exhibit a remarkable preference for the electron-rich alkynyl entities,[18,20,24,33,36−38] we still know very little about the factors controlling the final structures and properties of related Pt^{II}−Cd^{II} heterometallic systems.[19,21,29,30,39] For instance, we have found that $Cd(NO_3)_2$ reacts with $[cis\text{-}Pt(R_f)_2(C{\equiv}CR)_2]^{2-}$ ($R_f = C_6F_5$) to form $\{Pt_2Cd\}^{2-}$ species featuring only tweezer-like η^2-(alkyne)−Cd bonds.[29] However, while the dicationic "Cd(N−N)$_2^{2+}$" and "Cd(trpy)$^{2+}$" (trpy = 2,2′,6′,2″-terpyridine) units form bimetallic complexes in which the Cd^{II} contacts with both C^{α} atoms and the basic Pt^{II} (Pt···Cd 3.00−3.11 Å)[30] center, the "Cd(cyclen)$^{2+}$" unit affords a related complex $[cis\text{-}Pt(R_f)_2(C{\equiv}CPh)_2Cd(cyclen)]$ featuring a very short Pt→Cd bond (2.764(1) Å) and retaining only a weak interaction with one of the alkynyl fragments.[39]

Within this area some time ago[21] we found that $[Pt(C{\equiv}CPh)_4]^{2-}$ reacts with $Cd(ClO_4)_2\cdot 6H_2O$ to give an insoluble material of the expected stoichiometry $[PtCd(C{\equiv}CPh)_4]_n$ **A** as a white solid. However, attempts to obtain crystals of **A** only caused partial hydrolysis, yielding a very unusual decanuclear cluster $[Pt_4Cd_6(C{\equiv}CPh)_4(\mu\text{-}C{\equiv}CPh)_{12}(\mu_3\text{-}OH)_4]$ (yellow crystals) stabilized not only by bridging hydroxy groups but also by Pt···Cd and η^2-Cd−acetylide interactions.[21] As an extension of this work, we considered it to be of interest to study the neutralization reactions of other homoleptic derivatives $[Pt(C{\equiv}CAr)_4]^{2-}$ containing better electron donating alkynyl groups (Ar = Tol, C_6H_4OMe-4, C_6H_4OMe-3), with $Cd(ClO_4)_2\cdot 6H_2O$ and to investigate the reactivity of the resulting neutral Pt−Cd systems toward some nitrogen donor ligands with a twofold objective: (1) to prepare some new heterometallic homoleptic $\{Pt(C{\equiv}CR)_4Cd\}_n$ aggregates that enable a better characterization of this kind of systems, and (2) to obtain access to novel neutral alkynyl based $\{Pt(C{\equiv}CR)_4CdL_x\}_n$ compounds to know whether simple N-donor ligands would have any influence and be able to tune the luminescence properties.

In this contribution we report the preparation and optical properties of a series of some solvate $[Pt(C{\equiv}CR)_4Cd(S)]_2$ (**1(S)$_2$**, S = acetone, dmso) and unsolvated complexes $[Pt(C{\equiv}CR)_4Cd]_x$ **1′**, and a series of tetranuclear clusters $[Pt(C{\equiv}CR)_4CdL]_2$ (**2**−**5**, L = N donor). In addition, time-dependent density functional theory (TD-DFT) calculations were carried out on **1c(dmso)$_2$**, **2a**, **2c**, **4**, and **5**, with the aim of characterizing the highest few occupied and lowest few unoccupied molecular orbitals, thus gaining insight into the nature of their photophysical properties.

Experimental Section

Materials and Methods. All reactions were carried out under argon atmosphere using solvents from a solvent purification system (MBRAUW MB SPS-800). Elemental analyses were carried out with a Perkin-Elmer 2400 CHNS/O microanalyzer. IR spectra were recorded on a Nicolet Nexus FT-IR Spectrometer from Nujol mulls between polyethylene sheets. ^{1}H NMR spectra were recorded on a Bruker ARX 300 spectrometer; chemical shifts are reported in parts per million (ppm) relative

(11) For some reviews see: (a) Belluco, U.; Bertani, R.; Michelin, R. A.; Mozzon, M. *J. Organomet. Chem.* **2000**, *600*, 37. (b) Long, N. J.; Williams, C. K. *Angew. Chem., Int. Ed.* **2003**, *42*, 2586. (c) Bruce, M. I.; Low, P. J. *Adv. Organomet. Chem.* **2004**, *50*, 179. (d) Ren, T. *Organometallics* **2005**, *24*, 4854. (e) Akita, M.; Koike, T. *Dalton Trans.* **2008**, 3523. (f) Nguyen, P.; Gómez-Elipe, P.; Manners, I. *Chem. Rev.* **1999**, *99*, 1515. (g) Berenguer, J. R.; Lalinde, E.; Moreno, M. T. *Coord. Chem. Rev.* **2010**, *254*, 832.

(12) For some recent works see: (a) Rios, D.; Olmstead, M. M.; Balch, A. L. *Inorg. Chem.* **2009**, *48*, 5279. (b) Umakoshi, K.; Saito, K.; Arikawa, Y.; Onishi, M.; Ishizaka, S.; Kitamura, N.; Nakao, Y.; Sakaki, S. *Chem.—Eur. J.* **2009**, *15*, 4238. (c) Yue, C.; Yan, C.; Feng, R.; Wu, M.; Chen, L.; Jiang, F.; Hong, M. *Inorg. Chem.* **2009**, *48*, 2873. (d) Fernández, E. J.; Laguna, A.; López-de-Luzuriaga, J. M. *Dalton Trans.* **2007**, 1969. (e) Forniés, J.; García, A.; Lalinde, E.; Moreno, M. T. *Inorg. Chem.* **2008**, *47*, 3651. (f) Falvello, L. R.; Forniés, J.; Garde, R.; García, A.; Lalinde, E.; Moreno, M. T.; Steiner, A.; Tomás, M.; Usón, I. *Inorg. Chem.* **2006**, *45*, 2543. (g) Falvello, L. R.; Forniés, J.; Lalinde, E.; Menjón, B.; García-Monforte, M. A.; Moreno, M. T.; Tomás, M. *Chem. Commun.* **2007**, 3838. (h) Yam, V. W.-W.; Cheng, E. C.-C. *Chem. Soc. Rev.* **2008**, *37*, 1806. (i) Balch, A. L. **2007**, *123*, 1. (j) Kato, M. *Bull. Chem. Soc. Jpn.* **2007**, *80*, 287. (k) Katz, M. J.; Michaelis, V. K.; Aguiar, P. M.; Yson, R.; Lu, H.; Kaluarachchi, H.; Batchelor, R. J.; Schreckenbach, G.; Kroeker, S.; Patterson, H. H.; Leznoff, D. B. *Inorg. Chem.* **2008**, *47*, 6353. (l) Katz, M. J.; Ramnial, T.; Yu, H.-Z.; Leznoff, D. B. *J. Am. Chem. Soc.* **2008**, *130*, 10662. (m) Elbjeirami, O.; Omary, M. A. *J. Am. Chem. Soc.* **2007**, *129*, 11384. (n) Xia, B.-H.; Zhang, H.-X.; Che, C.-M.; Leung, K.-H.; Phillips, D. L.; Zhu, N.; Zhou, Z.-Y. *J. Am. Chem. Soc.* **2003**, *125*, 10362. (o) Gade, L. H. *Angew. Chem., Int. Ed.* **2001**, *40*, 3573.

(13) Eryazici, I.; Moorefield, C. N.; Newkome, G. R. *Chem. Rev.* **2008**, *108*, 1834.

(14) Yam, V. W.-W.; Chan, K. H.-Y.; Wong, K. M.-C.; Zhu, N. *Chem.—Eur. J.* **2005**, *11*, 4535.

(15) Koshevoy, I. O.; Lin, Y.-C.; Karttunen, A. J.; Haukka, M.; Chou, P.-T.; Tunik, S. P.; Pakkanen, T. A. *Chem. Commun.* **2009**, 2860.

(16) Wei, Q.-H.; Yin, G.-Q.; Zhang, L.-Y.; Shi, L.-X.; Mao, Z.-W.; Chen, Z.-N. *Inorg. Chem.* **2004**, *43*, 3484.

(17) Koshevoy, I. O.; Karttunen, A. J.; Tunik, S. P.; Haukka, M.; Selivanov, S. I.; Melnikov, A. S.; Serdobintsev, P. Y.; Pakkanen, T. A. *Organometallics* **2009**, *28*, 1369 and ref. therein.

(18) Charmant, J. P. H.; Forniés, J.; Gómez, J.; Lalinde, E.; Merino, R. I.; Moreno, M. T.; Orpen, A. G. *Organometallics* **1999**, *18*, 3353.

(19) Charmant, J. P. H.; Falvello, L. R.; Forniés, J.; Gómez, J.; Lalinde, E.; Moreno, M. T.; Orpen, A. G.; Rueda, A. *Chem. Commun.* **1999**, 2045.

(20) Ara, I.; Forniés, J.; Gómez, J.; Lalinde, E.; Moreno, M. T. *Organometallics* **2000**, *19*, 3137.

(21) Forniés, J.; Gómez, J.; Lalinde, E.; Moreno, M. T. *Inorg. Chem.* **2001**, *40*, 5415.

(22) Berenguer, J. R.; Forniés, J.; Gómez, J.; Lalinde, E.; Moreno, M. T. *Organometallics* **2001**, *20*, 4847.

(23) Berenguer, J. R.; Forniés, J.; Gil, B.; Lalinde, E. *Chem.—Eur. J.* **2006**, *12*, 785.

(24) Gil, B.; Forniés, J.; Gómez, J.; Lalinde, E.; Martín, A.; Moreno, M. T. *Inorg. Chem.* **2006**, *45*, 7788.

(25) Yam, V. W.-W.; Hui, C.-K.; Yu, S.-Y.; Zhu, N. *Inorg. Chem.* **2004**, *43*, 812.

(26) Yin, G.-Q.; Wei, Q.-H.; Zhang, L.-Y.; Chen, Z.-N. *Organometallics* **2006**, *25*, 580.

(27) Wei, Q.-H.; Yin, G.-Q.; Ma, Z.; Shi, L.-X.; Chen, Z.-N. *Chem. Commun.* **2003**, 2188.

(28) Yam, V. W.-W.; Yu, K.-L.; Cheung, K.-K. *J. Chem. Soc., Dalton Trans.* **1999**, 2913.

(29) Fernández, J.; Forniés, J.; Gil, B.; Gómez, J.; Lalinde, E.; Moreno, M. T. *Organometallics* **2006**, *25*, 2274.

(30) Berenguer, J. R.; Gil, B.; Fernández, J.; Forniés, J.; Lalinde, E. *Inorg. Chem.* **2009**, *48*, 5250.

(31) Ara, I.; Berenguer, J. R.; Forniés, J.; Gómez, J.; Lalinde, E.; Merino, R. I. *Inorg. Chem.* **1997**, *36*, 6461.

(32) Charmant, J. P. H.; Forniés, J.; Gómez, J.; Lalinde, E.; Merino, R. I.; Moreno, M. T.; Orpen, A. G. *Organometallics* **2003**, *22*, 652.

(33) Ara, I.; Berenguer, J. R.; Eguizábal, E.; Forniés, J.; Gómez, J.; Lalinde, E. *J. Organomet. Chem.* **2003**, *670*, 221.

(34) Berenguer, J. R.; Díez, A.; Fernández, J.; Forniés, J.; García, A.; Gil, B.; Lalinde, E.; Moreno, M. T. *Inorg. Chem.* **2008**, *47*, 7703.

(35) Forniés, J.; Fuertes, S.; Martín, A.; Sicilia, V.; Gil, B.; Lalinde, E. *Dalton Trans.* **2009**, 2224.

(36) Díez, A.; García, A.; Lalinde, E.; Moreno, M. T. *Eur. J. Inorg. Chem.* **2009**, 3060.

(37) Forniés, J.; Gómez, J.; Lalinde, E.; Moreno, M. T. *Inorg. Chim. Acta* **2003**, *347*, 145.

(38) Forniés, J.; Fuertes, S.; Martín, A.; Sicilia, V.; Lalinde, E.; Moreno, M. T. *Chem.—Eur. J.* **2006**, *12*, 8253.

(39) Forniés, J.; Ibáñez, S.; Martín, A.; Gil, B.; Lalinde, E.; Moreno, M. T. *Organometallics* **2004**, *23*, 3963.

to external tetramethylsilane, $SiMe_4$, and coupling constants in hertz (Hz). Complex **4** is the only soluble enough to register its ^{195}Pt NMR spectrum, being recorded on a Bruker ARX 400 spectrometer; chemical shift is reported in ppm relative to Na_2PtCl_6 in D_2O. UV−vis spectra were recorded on a Hewlet Packard 8453 spectrometer. Diffuse reflectance UV−vis (DRUV) data of pressed powder were recorded on a Shimazdu UV-3600 spectrophotometer with a Harrick praying mantis accessory, and recalculated following the Kubelka−Munk function. Excitation and emission spectra were obtained on a Jobin−Yvon Horiba Fluorolog 3−11 Tau-3 spectrofluorimeter. The lifetime measurements were performed operating in the phosphorimeter mode (with a F1−1029 lifetime emission PMT assembly, using a 450 W Xe lamp). Quantum yields in the solid state were measured upon excitation at 400 nm (**2a**, **2c**, **3**, and **4**), 420 nm (**2b**), or 430 nm (**5**) using a F-3018 Integrating Sphere mounted on a Fluorolog 3−11 Tau-3 spectrofluorimeter. Data were fittered using the Jobin−Yvon software package. $(NBu_4)_2[Pt(C{\equiv}CR)_4]$ (R = Tol, C_6H_4-OMe-4, C_6H_4OMe-3)[40] were prepared as reported, and other reagents were obtained from commercial sources.

Preparation of $[Pt(C{\equiv}CTol)_4Cd(acetone)]_2$ ($\mathbf{1a(acetone)_2}$). $Cd(ClO_4)_2\cdot 6H_2O$ (0.110 g, 0.262 mmol) was added to a colorless solution of $(NBu_4)_2[Pt(C{\equiv}CTol)_4]$ (0.300 g, 0.262 mmol) in acetone (10 mL), and the mixture stirred for 15 min. The yellow solid obtained **1a(acetone)$_2$** was filtered and washed with acetone (0.123 g, 56%). Anal. Calcd for $C_{78}H_{68}O_2Cd_2Pt_2$ (1652.38): C, 56.70; H, 4.15. Found: C, 56.96; H, 4.36. IR (cm^{-1}): ν(C≡C) 2120 (w), 2078 (sh), 2057 (m), 2025 (sh); ν(C=O) 1662 (s). ^1H NMR (δ, 300.13 MHz, $CDCl_3$): 7.37 (d, J = 7.6 Hz, 16H, C_6H_4, Tol); 6.94 (d, J = 7.6 Hz, 16H, C_6H_4, Tol); 2.17 (s, overlapping of 24H, CH_3, Tol and 12H, CH_3, CH_3COCH_3). ^1H NMR (δ, 300.13 MHz, CD_3COCD_3): 7.10 (d, J = 7.1 Hz, 16H, C_6H_4, Tol); 6.85 (d, J = 7.1 Hz, 16H, C_6H_4, Tol); 2.24 (s, 24H, CH_3, Tol). The low solubility of this complex precludes its characterization by $^{13}C\{^1H\}$ NMR.

Preparation of $[Pt(C{\equiv}CTol)_4Cd]_2$ (1a). Prolonged vacuum treatment (∼48 h) at ∼60° of the yellow solid **1a(acetone)$_2$** (0.123 g, 0.074 mmol) causes the elimination of acetone molecules giving complex **1a** as an orange-brown solid (0.114 g, 100%). Anal. Calcd for $C_{72}H_{56}Cd_2Pt_2$ (1536.22): C, 56.29; H, 3.67. Found: C, 56.50; H, 3.91. IR (cm^{-1}): ν(C≡C) 2054 (s). ^1H NMR (δ, 300.13 MHz, $CDCl_3$): 7.36 (d, J = 7.5 Hz, 16H, C_6H_4, Tol); 6.94 (d, J = 7.5 Hz, 16H, C_6H_4, Tol); 2.17 (s, 24H, CH_3, Tol). ^1H NMR (δ, 300.13 MHz, CD_3COCD_3): Shows the same pattern than **1a(acetone)$_2$**.

Preparation of $[Pt(C{\equiv}CTol)_4Cd]_x$ (1′a). 1a(acetone)$_2$ (0.100 g, 0.061 mmol) was treated with CH_2Cl_2 (∼ 15 mL) yielding a yellow solution. By stirring at room temperature ∼15 min a white solid $[Pt(C{\equiv}CTol)_4Cd]_x$ **1′a** separates (0.030 g, 32%). This solid is only soluble in dmso. Anal. Calcd for $C_{36}H_{28}CdPt$ (768.11): C, 56.29; H, 3.67. Found: 56.53; H, 3.99. IR(cm^{-1}): ν(C≡C) 2055 (s), 2023 (sh). ^1H NMR (δ, 300.13 MHz, d_6-dmso, yellow solution): 7.15 (d, J = 7.8 Hz, 8H, C_6H_4, Tol); 7.05 (d, J = 7.8 Hz, 8H, C_6H_4, Tol); 2.05 (s, 12H, CH_3, Tol).

Reaction of $(NBu_4)_2[Pt(C{\equiv}CC_6H_4OMe\text{-}4)_4]$ with $Cd(ClO_4)\cdot 6H_2O$. The reaction of $(NBu_4)_2[Pt(C{\equiv}CC_6H_4OMe\text{-}4)_4]\cdot 2H_2O$ (0.300 g, 0.242 mmol) in acetone (∼10 mL) and $Cd(ClO_4)_2\cdot 6H_2O$ (0.101 g, 0.242 mmol) was analogous to the previously described one causing the precipitation of a yellow solid which was filtered, washed with acetone, and air-dried, yielding $[Pt(C{\equiv}CC_6H_4OMe\text{-}4)_4Cd(acetone)]_2$ **1b(acetone)$_2$** as a deep yellow solid (0.115 g, 56%). Prolonged (∼3 h) vacuum treatment at ∼40 °C causes the loss of the acetone molecules yielding **1b** as a brown-orange solid. The yellow **1b(acetone)$_2$** or brown-orange **1b** solids dissolve in CH_2Cl_2 yielding an initial yellow solution from which gradually precipitates $[Pt(C{\equiv}CC_6H_4OMe\text{-}4)_4Cd]_x$ **1′b** as a white solid with high yield (∼ 90%).

Data for **1b(acetone)$_2$**: Anal. Calcd for $C_{78}H_{68}O_{10}Cd_2Pt_2$ (1780.37): C, 52.62; H, 3.85. Found: C, 51.92; H, 3.15. IR (cm^{-1}): ν(C≡C) 2095 (sh), 2057 (m), 2018 (sh), 1987 (sh); ν(C=O) 1691 (s). ^1H NMR (δ, 300.13 MHz, $CDCl_3$): 7.43 (d, J = 7.8 Hz, 16H, C_6H_4, C_6H_4OMe-4); 6.67 (d, J = 7.8 Hz, 16H, C_6H_4, C_6H_4OMe-4); 3.57 (s, 24H, OCH_3, C_6H_4OMe-4); 2.17 (s, 12H, CH_3COCH_3).

Data for **1b**: Anal. Calcd for $C_{72}H_{56}O_8Cd_2Pt_2$ (1664.21): C, 51.96; H, 3.39; Found: C, 51.85; H, 3.10. IR (cm^{-1}): ν(C≡C) 2053 (s), 2027 (sh). ^1H NMR (δ, 300.13 MHz, CD_2Cl_2): 7.41 (dbr, J ∼ 8.5 Hz, 16H, C_6H_4, C_6H_4OMe-4); 6.68 (d, J = 8.5 Hz, 16H, C_6H_4, C_6H_4OMe-4); 3.57 (s, 24H, OCH_3, C_6H_4OMe-4).

Data for **1′b**: Anal. Calcd for $C_{36}H_{28}O_4CdPt$ (832.11): C, 51.96; H, 3.39; Found: C, 51.85; H, 3.22. IR (cm^{-1}): 2055 (s), 2029 (sh). ^1H NMR (δ, 300.13 MHz, d_6-dmso, yellow solution): 7.20 (d, J = 8.4 Hz, 16H, C_6H_4, C_6H_4OMe-4); 6.82 (d, J = 8.4 Hz, 16H, C_6H_4, C_6H_4OMe-4); 3.72 (s, 24H, OCH_3, C_6H_4OMe-4).

Preparation of $[Pt(C{\equiv}CC_6H_4OMe\text{-}3)_4Cd]_x$ (1′c). $Cd(ClO_4)_2\cdot 6H_2O$ (0.104 g, 0.248 mmol) was added to a solution of $(NBu_4)_2[Pt(C{\equiv}CC_6H_4OMe\text{-}3)_4]$ (0.300 g, 0.248 mmol) in acetone (∼15 mL), and the mixture was stirred for 15 min. In this case, complex **1′c** precipitated as a final cream-white solid which was filtered, washed with acetone and air-dried (0.145 g, 70%). Anal. Calcd for $C_{36}H_{28}O_4CdPt$ (832.11): C, 51.96; H, 3.39. Found 51.57; H, 3.42. IR (cm^{-1}): ν (C≡C) 2040 cm^{-1} (m). ^1H NMR (δ, 300.13 MHz, d_6-dmso, yellow solution): 7.12 (t, J = 7.7 Hz, $4H^5$, C_6H_4OMe-3); 6.86 (d, J = 7.3 Hz, $4H^{4\text{ or }6}$, C_6H_4O-Me-3); 6.81 (s, $4H^2$, C_6H_4OMe-3); 6.73 (d, J = 7.5 Hz, $4H^{4\text{ or }6}$, C_6H_4OMe-3); 3.72 (s, 12H, OCH_3, C_6H_4OMe-3). Not soluble enough for $^{13}C\{1H\}$ NMR.

Preparation of $[Pt(C{\equiv}CTol)_4Cd(py)]_2$ (2a). A solution of complex **1a(acetone)$_2$** (0.150 g, 0.091 mmol) in CH_2Cl_2 was treated with excess of pyridine (500 μL, 6.20 mmol). Slow evaporation of the resulting bright yellow solution at 0° generates yellow-greenish crystals of **2a** (0.115 g, 75%). Anal. Calcd for $C_{82}H_{66}N_2Cd_2Pt_2$ (1694.42): C, 58.13; H, 3.93; N, 1.65. Found: C, 58.02; H, 3.92; N, 1.60. IR (cm^{-1}): ν(C≡C) 2108 (w), 2094 (sh), 2084 (s). $\Lambda_M(CH_2Cl_2)$: ∼ 0 $\Omega^{-1}\cdot cm^2\cdot mol^{-1}$. ^1H NMR (δ, 300.13 MHz, $CDCl_3$): 8.92 (sbr, $4H^{2,6}$, py); 7.66 (t, J = 7.4 Hz, $2H^4$, py); 7.17 (m, $4H^{3,5}$, py); 6.84 (d, J = 7.5 Hz, 16H, C_6H_4, Tol); 6.59 (d, J = 7.5 Hz, 16H, C_6H_4, Tol); 2.14 (s, 24H, CH_3, Tol). The low solubility of this complex precludes its characterization by $^{13}C\{^1H\}$ NMR.

Preparation of $[Pt(C{\equiv}CC_6H_4OMe\text{-}4)_4Cd(py)]_2$ (2b). This complex was prepared in a similar way to complex **2a** starting from $[Pt(C{\equiv}CC_6H_4OMe\text{-}4)_4Cd]_2$ **1b** (0.150 g, 0.090 mmol) and pyridine (500 μL, 6.20 mmol). The resulting yellow mixture was stirred for 30 min at room temperature, and the yellow solid thus obtained **2b** was filtered, washed with CH_2Cl_2, and dried in vacuum (0.140 g, 85%). A similar result is obtained starting from **1b(acetone)$_2$**. Anal. Calcd for $C_{82}H_{66}N_2O_8Cd_2Pt_2$ (1822.41): C, 54.04; H, 3.65; N, 1.54. Found: C, 53.92; H, 3.42; N, 1.78. IR (cm^{-1}): ν(C≡C) 2112 (sh), 2085 (m). ^1H NMR (δ, 300.13 MHz, d_6-dmso): 8.58 (d, J = 4.19 Hz, $4H^{2,6}$, py); 7.78 (t, J = 7.7 Hz, $2H^4$, py); 7.38 (dd, J = 5.6; 7.7 Hz; $4H^{3,5}$, py); 7.20 (d, J = 8.6 Hz, 16H, C_6H_4, C_6H_4OMe-4); 6.82 (d, J = 8.6 Hz, 16H, C_6H_4, C_6H_4OMe-4); 3.72 (s, 24H, OCH_3, C_6H_4OMe-4). $^{13}C\{^1H\}$ NMR: not soluble enough.

Preparation of $[Pt(C{\equiv}CC_6H_4OMe\text{-}3)_4Cd(py)]_2$ (2c). A white suspension of $[\{Pt(C{\equiv}CC_6H_4OMe\text{-}3)_4\}Cd]_x$ (**1′c**) (0.150 g, 0.180 mmol) was treated with excess of pyridine (500 μL, 6.20 mmol). Slow evaporation of the resulting bright yellow solution at 0 °C generates yellow-greenish crystals of **2c** (0.090 g, 55%). Anal. Calcd for $C_{82}H_{66}N_2O_8Cd_2Pt_2$ (1822.41): C, 54.04; H, 3.65; N, 1.54. Found C, 53.82; H, 3.57; N, 1.75. IR (cm^{-1}): ν(C≡C) 2086 (m). ^1H NMR (δ, 300.13 MHz, CD_2Cl_2): 8.83 (s, $4H^{2,6}$, py); 7.70 (t, J = 7.7 Hz, $2H^4$, py); 7.24 (st, J ∼ 6.7 Hz; $4H^{3,5}$, py); 6.72

(40) Benito, J.; Berenguer, J. R.; Forniés, J.; Gil, B.; Gómez, J.; Lalinde, E. *Dalton Trans.* **2003**, 4331.

(t, J = 7.5 Hz, 8H^5, C_6H_4, C_6H_4OMe-3); 6.56−6.50 (m, 24H, C_6H_4, C_6H_4OMe-3); 3.44 (s, 24H, OCH_3, C_6H_4OMe-3). $^{13}C\{^1H\}$ NMR: not soluble enough.

Preparation of [Pt(C≡CTol)$_4$Cd(NC$_5$H$_4$CH$_3$-4)]$_2$ (3). This complex was prepared in a similar way to complex **2a** starting from **1a(acetone)$_2$** (0.200 g, 0.121 mmol) and excess of NC_5H_4-CH_3-4 (500 μL, 5.10 mmol). In this case, **3** precipitated as a pale yellow microcrystalline solid (0.193 g, 93%). Anal. Calcd for $C_{84}H_{70}N_2Cd_2Pt_2$ (1722.47): C, 58.57; H, 4.10; N, 1.63. Found: C, 58.53; H, 4.05; N, 1.51. IR (cm^{-1}): ν(C≡C) 2102 (sh), 2094 (sh), 2085 (s). $\Lambda_M(CH_2Cl_2)$: ∼ 0 $\Omega^{-1}\cdot cm^2\cdot mol^{-1}$. ^{1}H NMR ($\delta$, 300.13 MHz, $CDCl_3$): 8.73 (sbr, 4H^{2,6}, $NC_5H_4CH_3$-4); 6.94 (bs, J = 7.4 Hz, 4H^{3,5}, $NC_5H_4CH_3$-4); 6.87 (d, J = 7.8 Hz, 16H, C_6H_4, Tol); 6.61 (d, J = 7.8 Hz, 16H, C_6H_4, Tol); 2.28 (s, 6H, CH_3, $NC_5H_4CH_3$-4); 2.16 (s, 24H, CH_3, Tol). The low solubility of this complex precludes its characterization by $^{13}C\{^1H\}$ NMR.

Preparation of [Pt(C≡CTol)$_4$Cd(NC$_5$H$_4$CF$_3$-4)]$_2$ (4). Excess of $NC_5H_4CF_3$-4 (1000 μL, 7.98 mmol) was added to a solution of [Pt(C≡CTol)$_4$Cd(acetone)]$_2$ **1a(acetone)$_2$** (0.205 g, 0.124 mmol) in 10 mL of CH_2Cl_2. The resulting yellow solution was kept at −30° for 3 days, affording greenish yellow crystals of **4** (0.100 g, 44%). Anal. Calcd for $C_{84}H_{64}N_2F_6Cd_2Pt_2$ (1830.39): C, 55.12; H, 3.52; N, 1.53. Found: C, 54.79; H, 3.41; N, 1.30. IR (cm^{-1}): ν(C≡C) 2115 (s), 2089 (s), 2069 (m). $\Lambda_M(CH_2Cl_2)$: ∼ 0 $\Omega^{-1}\cdot cm^2\cdot mol^{-1}$. ^{1}H NMR ($\delta$, 300.13 MHz, $CDCl_3$, equilibrium mixture of **1a** and **4** in about molar ratio 3:2): 8.89 (d, J = 4.4 Hz, 4H^{2,6}, $NC_5H_4CF_3$-4); ∼ 7.35 (d, 13H, H^{3,5} of $NC_5H_4CF_3$-4 overlapped with d, C_6H_4, Tol, **1a**); 6.93 (d, J = 7.4 Hz, 9H, C_6H_4, Tol, **1a**); 6.88 (d, $J \approx$ 7.9 Hz, 7H, C_6H_4, Tol, **4**); 6.65 (d, $J \approx$ 7.9 Hz, 7H, C_6H_4, Tol, **4**); 2.17 (s, 24H, CH_3, Tol, **1a** and **4**). ^{1}H NMR of **4** + $NC_5H_4CF_3$-4 (6 equiv) (δ, 300.13 MHz, $CDCl_3$): 8.87 (d, J = 4.9 Hz, H^{2,6}, $NC_5H_4CF_3$-4); ∼ 7.42 (d, H^{3,5}, $NC_5H_4CF_3$-4); 7.00 (d, J = 7.8 Hz, C_6H_4, Tol); 6.54 (d, J = 7.8 Hz, C_6H_4, Tol); 2.17 (s, 6H, CH_3, Tol). ^{195}Pt NMR of **4** + $NC_5H_4CF_3$-4 (6 equiv) (δ, 85.68 MHz, CD_2Cl_2): −3761 (s, $^1J(^{195}Pt-^{111}Cd)$ = 1855 Hz, $^1J(^{195}Pt-^{113}Cd)$ = 1941 Hz). The low solubility of this complex precludes its characterization by $^{13}C\{^1H\}$ NMR.

Preparation of [Pt(C≡CTol)$_4$Cd(pzH)]$_2$ (5). A CH_2Cl_2 (10 mL) solution of **1a(acetone)$_2$** (0.200 g, 0.121 mmol) was treated with pzH (0.018 g, 0.264 mmol). Then, acetone (∼ 10 mL) was added to the resulting yellow solution, and the mixture was slowly evaporated at 0 °C generating yellow crystals with stoichiometry **5**·2acetone (0.180 g, 83%). Anal. Calcd for $C_{78}H_{64}N_4Cd_2Pt_2\cdot 2C_3H_6O$ (1788.53): C, 56.41; H, 4.28; N, 3.13. Found: C, 56.31; H, 3.86; N, 3.50. IR (cm^{-1}): ν(N−H) 3600 (m), 3462 (m); ν(C≡C) 2112 (sh), 2104 (sh), 2096 (m), 2081 (m), 2061 (sh); $\nu(C{=}O)_{acetone}$ 1607 (m). $\Lambda_M(CH_2Cl_2)$: ∼ 0 $\Omega^{-1}\cdot cm^2\cdot mol^{-1}$. ^{1}H NMR ($\delta$, 300.13 MHz, CD_2Cl_2): 11.97 (sbr, 2NH, pzH); ∼ 7.3 (br, 4H^{3,5}, pzH); 6.84 (16H), 6.74 (16H) (AB system, J = 7.8 Hz, C_6H_4, Tol); 6.27 (pt, J = 2.4 Hz, 2H^4, pzH), 2.20 (s, 24H, CH_3, Tol); 2.10 (s, 12H, CH_3COCH_3). Upon cooling, the resonance due to H^3 and H^5 broadens ($T_{coalescence} \sim$ 293 K) and finally splits (∼ 282 K), and the $\delta H_A - \delta H_B$ separation of the AB system (C_6H_4, Tol) becomes gradually smaller, collapsing into a singlet at 223 K. Data at 223 K: 12.00 (s, 2NH, pzH); 7.50 (s, 2H^5, pzH); 7.17 (s, 2H^3, pzH); 6.71 (s, 32H, C_6H_4, Tol); 6.30 (s, 2H^4, pzH); 2.16 (s, 24H, CH_3, Tol); 2.01 (s, 12H, CH_3COCH_3). $\Delta G^{\ddagger}_{293}$ for H^3,H^5 interconversion ≈58.43 kJ mol^{-1}. The low solubility of this complex precludes its characterization by $^{13}C\{^1H\}$.

Computational Details for DFT Calculations. All calculation on complexes **1c(dmso)$_2$**, **2a**, **2c**, **4**, and **5** were carried out using the molecular geometry obtained through X-ray diffraction analysis. Keeping all distances, angles, and dihedral angles frozen, single point density functional theory (DFT) calculations with the Gaussian03[41] program were performed, using Becke's three-parameter functional combined with Lee−Yang−Parr's correlation functional[42−44] (B3LYP). The basis set used was the LanL2DZ[45] effective core potential for the metal centers and 6-31G(d,p) for the ligand atoms. The time-dependent density-functional theory (TD-DFT) calculation was carried out using the polarized continuum model approach implemented in the Gaussian 03 software. Percentage compositions of molecular orbitals were calculated using the AOMix program.[46,47]

X-ray Crystallography. Details of the structural analyses for all complexes are summarized in Table 1. Yellow crystals of **1c(dmso)$_2$** were obtained by slow diffusion of Et_2O into a saturated solution of **1′c** in dmso/CH_2Cl_2 1:1. For **2a**, **2c**, and **5**, yellow crystals were grown by slow evaporation at 0 °C of the corresponding solutions of the complexes in CH_2Cl_2 (**2a**, **2c**) or CH_2Cl_2/acetone 1:1 (**5**). Finally, greenish yellow crystals of **4** were obtained by cooling a mixture of **4** and $NC_5H_4CF_3$-4 at −30 °C in CH_2Cl_2. One (**1c(dmso)$_2$**, **2a**) or 0.5 (**2c**, **4**) molecules of CH_2Cl_2 and one molecule of acetone (**5**) were found in the corresponding asymmetric units. Furthermore, for **5**, the existence of weak hydrogen interactions between the N−H of the pyrazole ligand and the oxygen atom of the acetone was confirmed. X-ray intensity data were collected with a NONIUS-κCCD area-detector diffractometer, using graphite-monochromatic Mo−K_α radiation. Images were processed using the DENZO and SCALEPACK suite of programs,[48] and the structures were solved by Direct Methods using SHELXS-97.[49] The absorption correction was performed using MULTI-SCAN[50] (**2a**, **2c**, **4** and **1c(dmso)$_2$**) or XABS2[51] (**5**), with the WINGX program suite.[52] The structures were refined by full-matrix least-squares on F^2 with SHELXL-97,[49] and all non-hydrogen atoms were assigned anisotropic displacement parameters. For complex **5**, the correct assignment of the position for the N(N−H) atom of the pzH ligand was confirmed by examination of the ΔMSDA values for bonds involving these atoms,[53,54] after refining the structure in three different ways (with the identities of the C and N in one position, reversed, and with 50/50 hybrid scattering factor at each of the affected atomic sites). The hydrogen atoms were constrained to idealized geometries fixing isotropic displacement parameters 1.2 times the U_{iso} value of their attached carbon for the aromatic and 1.5 times for the methyl groups. Several restraints have been used to model the CH_2Cl_2 molecule in **1c(dmso)$_2$** and the positional disorder presented by

(41) Frisch, M. J.; Trucks, G. W.; Schlegel, H. B.; Scuseria, G. E.; Robb, M. A.; Cheeseman, J. R.; Montgomery, J. A., Jr.; Vreven, T.; Kudin, K. N.; Burant, J. C.; Millam, J. M.; Iyengar, S. S.; Tomasi, J.; Farkas, O.; Tomasi, J.; Barone, V.; Mennucci, B.; Cossi, M.; Scalmani, G.; Rega, N.; Petersson, G. A.; Nakatsuji, H.; Hada, M.; Ehara, M.; Toyota, K.; Fukuda, R.; Hasegawa, J.; Ishida, M.; Nakajima, T.; Honda, Y.; Kitao, O.; Nakai, H.; Klene, M.; Li, X.; Knox, J. E.; Hratchian, H. P.; Cross, J. B.; Bakken, V.; Adamo, C.; Jaramillo, J.; Gomperts, R.; Stratman, R. E.; Yazyev, O.; Austin, A. J.; Cammi, R.; Pomelli, C.; Ochterski, J. W.; Ayala, P. Y.; Morokuma, K.; Voth, G. A.; Salvador, P.; Dannenberg, J. J.; Zakrzewski, V. G.; Dapprich, S.; Daniels, A. D.; Strain, M. C.; Farkas, O.; Malick, D. K.; Rabuck, A. D.; Raghavachari, K.; Foresman, J. B.; Ortiz, J. V.; Cui, Q.; Baboul, A. G.; Clifford, S.; Cioslowski, J.; Stefanov, B. B.; Liu, G.; Liashenko, A.; Piskorz, P.; Komaromi, I.; Martin, R. L.; Fox, D. J.; Keith, T.; Al-Laham, M. A.; Peng, C. Y.; Nanayakkara, A.; Challacombe, M.; Gill, P. M. W.; Johnson, B.; Chen, W.; Wong, M. W.; Gonzalez, C.; Pople, J. A. *Gaussian 03*, Revision E.01; Gaussian, Inc.: Wallingford, CT, 2004.

(42) Becke, A. D. *Phys. Rev. A: At., Mol., Opt. Phys* **1988**, *38*, 3098.
(43) Lee, C.; Yang, W.; Parr, R. G. *Phys. Rev. B: Condens. Mater. Phys.* **1988**, *B37*, 785–789.
(44) Becke, A. D. *J. Chem. Phys.* **1993**, *98*, 5648.
(45) Wadt, W. R.; Hay, P. J. *J. Chem. Phys.* **1985**, *82*, 284–298.
(46) Gorelsky, S. I. *AOMix: Program for Molecular Orbital Analysis*; University of Ottawa: Ottawa, Ontario, Canada, 2009; http://www.sg-chem.net/.
(47) Gorelsky, S. I.; Lever, A. B. P. *J. Organomet. Chem.* **2001**, *635*, 187.
(48) Otwinowski, Z.; Minor, W. *Methods Enzymol.* **1997**, *276*, 307.
(49) Sheldrick, G. M. *SHELX-97, a program for the refinement of crystal structures*; University of Göttingen: Göttingen, Germany, 1997.
(50) Blessing, R. H. *Acta Crystallogr.* **1995**, *A51*, 33.
(51) Parkin, S.; Moezzi, B.; Hope, H. *J. Appl. Crystallogr.* **1995**, *28*, 53.
(52) Farrugia, L. J. *J. Appl. Crystallogr.* **1999**, *32*, 837.
(53) Speck, A. L. *Acta Crystallogr., Sect. A.* **1990**, *46*, c34.
(54) Hirshfeld, F. L. *Acta Crystallogr., Sect. A.* **1976**, *32*, 239.

Table 1. Crystallographic Data for **1c(dmso)$_2$**·2CH_2Cl_2, **2a**·2CH_2Cl_2, **2c**·CH_2Cl_2, **4**·CH_2Cl_2, and **5**·2 Acetone

	1c(dmso)$_2$·2CH_2Cl_2	**2a**·2CH_2Cl_2	**2c**·CH_2Cl_2
empirical formula	$C_{78}H_{72}Cd_2Cl_4O_{10}Pt_2S_2$	$C_{42}H_{35}CdCl_2NPt$	$C_{83}H_{68}Cd_2Cl_2N_2O_8Pt_2$
F_w	1990.26	932.10	1907.27
T (K)	173(1)	173(1)	173(1)
crystal system, space group	monoclinic, $P2_1/n$	triclinic; $P\bar{1}$	monoclinic, $P2_1/n$
a(Å)	13.3388(4)	9.8650(2)	14.4841(4)
b(Å)	14.4103(8)	13.8180(3)	13.1672(4)
c(Å)	20.8566(12)	14.4500(3)	20.6477(3)
α(deg)	90	69.9970(10)	90
β(deg)	108.259(3)	81.6860(10)	91.4520(10)
γ(deg)	90	89.4250(10)	90
volume (A^3)	3807.1(3)	1829.82(7)	3936.56(17)
Z	2	2	2
D_{calcd} (Mg/m^3)	1.736	1.692	1.609
absorption coefficient (mm^{-1})	4.465	4.575	4.197
F(000)	1944	908	1860
θ range for data collection (deg)	3.25 to 25.68	2.09 to 27.89	3.38 to 25.68
no of data/restraints/params	7202/5/442	8671/0/437	7445/0/464
goodness-of-fit on F^2 [a]	1.011	1.016	1.025
final R indexes [$I > 2\sigma(I)$][a]	R1 = 0.0586, wR2 = 0.1232	R1 = 0.0347, wR2 = 0.0690	R1 = 0.0302, wR2 = 0.0776
R indexes (all data)[a]	R1 = 0.1129, wR2 = 0.1442	R1 = 0.0491, wR2 = 0.0730	R1 = 0.0399, wR2 = 0.0827
largest diff peak and hole (e.Å $^{-3}$)	1.681 and −1.360	1.015 and −1.138	1.704 and −0.980

	4·CH_2Cl_2	**5**·2acetone
empirical formula	$C_{85}H_{66}Cd_2Cl_2F_6N_2Pt_2$	$C_{42}H_{38}CdN_2OPt$
F_w	1915.28	894.23
T (K)	173(1)	173(1)
crystal system, space group	monoclinic, C2/c	triclinic; $P\bar{1}$
a(Å)	17.9732(5)	9.6288(4)
b(Å)	26.8534(8)	13.8741(5)
c(Å)	15.9466(4)	14.3504(6)
α(deg)	90	71.144(2)
β(deg)	102.5110(10)	80.783(2)
γ(deg)	90	87.744(2)
volume (A^3)	7513.7(4)	1790.62(12)
Z	4	2
D_{calcd} (Mg/m^3)	1.693	1.659
absorption coefficient (mm^{-1})	4.402	4.530
F(000)	3720	876
θ range for data collection (deg)	3.53 to 27.10	2.95 to 25.68
no of data/restraints/params	8276/6/454	6666/0/431
goodness-of-fit on F^2 [a]	1.039	1.025
final R indexes [$I > 2\sigma(I)$][a]	R1 = 0.0285, wR2 = 0.0654	R1 = 0.0455, wR2 = 0.1195
R indexes (all data)[a]	R1 = 0.0378, wR2 = 0.0698	R1 = 0.0483, wR2 = 0.1225
largest diff peak and hole (e Å^{-3})	1.109 and −1.360	2.623 and −2.553

[a] $R1 = \sum||F_o| - |F_c||/\sum|F_o|$; $wR2 = [\sum w(F_o^2 - F_c^2)^2/\sum w(F_o^2)^2]^{1/2}$; goodness of fit $= \{\sum[w(F_o^2 - F_c^2)^2]/(N_{obs} - N_{param})\}^{1/2}$; $w = [\sigma^2(F_o) + (g_1P)^2 + g_2P]^{-1}$; $P = [\max(F_o^2;0 + 2F_c^2]/3$.

the CF_3 group of the $NC_5H_4CF_3$-4 ligand in **4**. Finally, all the structures show some residual peaks greater than 1 e A^{-3} in the vicinity of the platinum atoms or solvent molecules, but with no chemical meaning.

Results and Discussion

Synthesis and Spectroscopic Characterization. As is shown in Scheme 1, the reaction of $[Pt(C{\equiv}CR)_4]^{2-}$ with cadmium perchlorate depends on the R substituent. Thus, treatment of the tolyl- and *p*-methoxyphenyl-alkynyl platinum(II) derivatives with Cd^{2+} in acetone leads to the formation of solvate complexes of stoichiometry $[Pt(C{\equiv}CR)_4Cd(acetone)]_2$ **1a,b(acetone)$_2$** (R = Tol **a**, C_6H_4OMe-4 **b**) as bright yellow solids. By contrast, a similar reaction starting from $(NBu_4)_2[Pt(C{\equiv}CC_6H_4OMe\text{-}3)_4]$ results in the precipitation of a solvent-free species $[Pt(C{\equiv}CC_6H_4OMe\text{-}3)_4Cd]_x$ **1′c** as a white solid. The acetone solvate **1a,b(acetone)$_2$** dissolve only in chlorinated solvents (CH_2Cl_2, $CHCl_3$) allowing their characterization by ^{1}H NMR in $CDCl_3$ solution (freshly prepared solution, see Experimental Section). However, in solution these species are unstable, evolving to free-acetone species $[Pt(C{\equiv}CR)_4Cd]_x$ (R = Tol **1′a**; R = C_6H_4OMe-4 **1′b**), which are similar to **1′c**, and gradually precipitating (∼15 min) as white powders.

All attempts to obtain crystals of either the solvate **1a,b(acetone)$_2$** or the free solvent **1′a**−**c** species failed. The most significant and distinctive spectroscopic feature is observed in their IR spectra. Thus, the IR spectra of the solvate complexes **1a,b(acetone)$_2$** exhibit several ν(C≡C) bands (2120, 2078 (sh), 2057, 2025 (sh) **1a(acetone)$_2$**; 2095 (sh), 2057, 2018 (sh) cm^{-1} **1b(acetone)$_2$**) consistent with the presence of different alkynyl coordination modes (terminal and bridging). This pattern is comparable to that observed for the tetranuclear derivatives (**2a**,**b**,**3**−**5**), suggesting that these solvates have, in the solid state, a tetranuclear sandwich structure $[Pt(C{\equiv}CR)_4Cd(acetone)]_2$ **1a,b(acetone)$_2$**, similar to those found for **1c(dmso)$_2$** and **2**−**5**, in which the acetone molecules are bonded to the Cd center (see Scheme 1). By contrast, the free-solvent derivatives **1′a**−**c** exhibit one ν(C≡C) band (with a shoulder in **1′a** and **1′b**) in the typical range of η^2-alkynyl bridging ligands (2055, 2023 (sh) cm^{-1} **1′a**; 2055, 2029 (sh) cm^{-1} **1′b**; 2040 cm^{-1} **1′c**).

Scheme 1

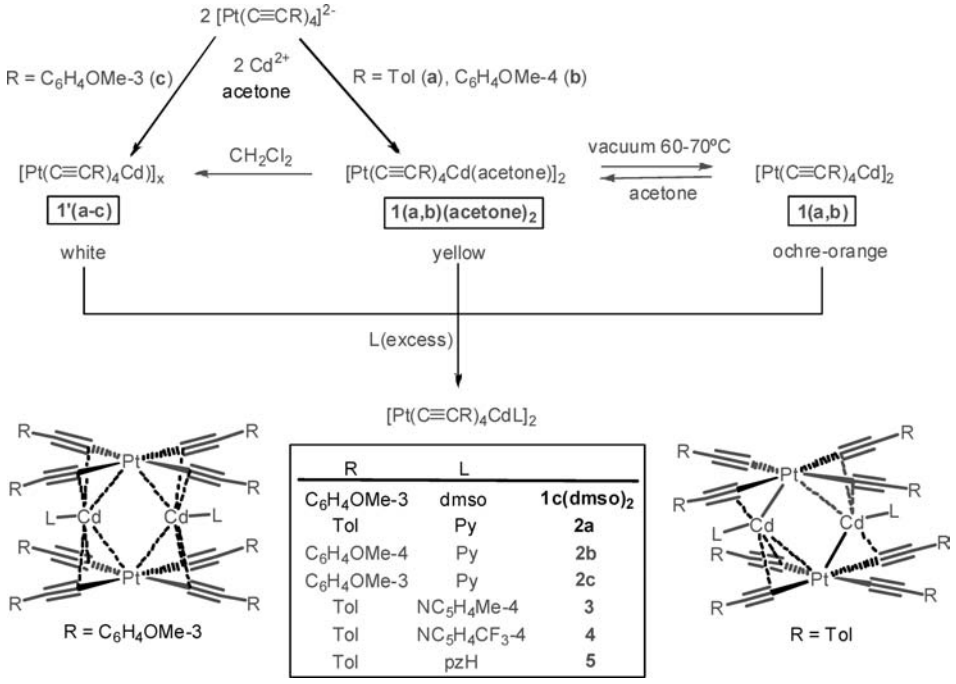

R	L	
C_6H_4OMe-3	dmso	**1c(dmso)$_2$**
Tol	Py	**2a**
C_6H_4OMe-4	Py	**2b**
C_6H_4OMe-3	Py	**2c**
Tol	NC_5H_4Me-4	**3**
Tol	$NC_5H_4CF_3$-4	**4**
Tol	pzH	**5**

This spectroscopic feature, together with their white color and null solubility in common polar and/or weak donor organic solvents (CH_2Cl_2, $CHCl_3$, CH_3COCH_3, THF, NCMe), suggest that they are presumably of polymeric nature. It is likely that, in the final free-acetone species **1′a**−**c**, the Cd^{II} ions shift toward an "*in-plane*" bis-(η^2-alkyne) tweezer-like coordination, in such a way that each platinate fragment acts as bis-(chelating) bridging ligand between consecutive cadmium centers. The stabilization of a naked Cd^{II} ion by four η^2 alkynyl ligands has been recently found in the trinuclear anions $[\{(R_f)_2Pt(\mu\text{-}C{\equiv}CR)_2\}_2Cd]^{2-}$ ($R_f = C_6F_5$).[29] Curiously complexes **1′a**−**c** proved to be only slightly soluble in d_6-dimethylsulfoxide, allowing their characterization by ^1H NMR spectroscopy (see Experimental Section). However, in this strong donor solvent the color of the white solids change to yellow, and the small amount that is dissolved (with sonication) yielded deep-yellow solutions, thus indicating that the $(CH_3)_2SO$ molecules interact with the cadmium centers stabilizing tetranuclear species $[Pt(C{\equiv}CR)_4Cd(dmso)]_2$ analogous to complexes **2**−**5**. Fortunately, after many attempts a few yellow crystals suitable for X-ray could be obtained by slow diffusion of Et_2O into a saturated dmso/CH_2Cl_2 solution of **1′c**, confirming the formation of the solvate $[Pt(C{\equiv}CC_6H_4OMe\text{-}3)_4Cd(dmso)]_2$ **1c(dmso)$_2$**.

Tetranuclear aggregates $[Pt(C{\equiv}CR)_4CdL]_2$ (L = py; R = Tol **2a**, C_6H_4OMe-4 **2b**, C_6H_4OMe-3 **2c**. R = Tol; L = $NC_5H_4CH_3$-4 **3**, $NC_5H_4CF_3$-4 **4**, $N_2C_3H_4$ (pzH) **5**) were easily synthesized by treatment of either the acetone solvate **1a,b(acetone)$_2$** or the polymeric **1′a**−**c** species with the corresponding N-donor ligand. It is worth noting that the same products are obtained even if a large excess of the corresponding ligand is used, indicating the strong bonding preference of Cd^{II} for the platinum alkyne fragments. The complexes were isolated as yellow crystals (**2a**, **2c**, **4**, **5**) or microcrystalline yellow powder (**2b**, **3**), and their identities were confirmed by microanalysis and spectroscopic means. The IR spectra of **2a**,**b**, **3**−**5** show several $\nu(C{\equiv}C)$ stretching bands in the 2115−2069 cm^{-1} range, in agreement with the presence of terminal and different unsymmetric bridging ligands, while one $\nu(C{\equiv}C)$ stretching band is found (2086 cm^{-1}) in the spectrum of **2c**, which is consistent with the presence of only one type of bridging alkynyl ligand, all these facts being confirmed by X-ray crystallography.

Because of the low solubility of these complexes, only the ^1H and ^{195}Pt (for **4**) could be recorded. In particular, **2b** is only soluble in d^6-dmso, but in this strong donor solvent the ^1H NMR pattern reveals (see Experimental Section) the presence of free pyridine and an identical AB pattern for the aryl C_6H_4OMe-4 protons to that seen for the precursor **1′b** in d^6-dmso, suggesting that similar $[Pt(C{\equiv}CC_6H_4OMe\text{-}4)_4Cd(dmso)]_2$ species are present in this solvent. Complexes **2a,c** and **3** dissolve in CD_2Cl_2 (**2c**) or $CDCl_3$ (**2a**, **3**) and both the *low* field shifts of the pyridine *ortho* protons ($\Delta H^{2,6} = 0.46$ **2a**; 0.27 ppm **2c**, **3**) and the pattern of the aryl C_6H_4R protons, shifted to low frequencies in relation to $[Pt(C{\equiv}CC_6H_4R)_4]^{2-}$, support that the tetranuclear aggregates retain their integrity in solution. Complexes **4** and **5** are found to be involved in dynamic processes. In the case of **4**, and probably because of the lower basicity of the $NC_5H_4CF_3$-4 ligand, its proton spectrum ($CDCl_3$) shows the presence of an equilibrium mixture of the precursor **1a** and **4** (δ 6.88, 6.65; AB system C_6H_4Me-4) in about a molar ratio of 3:2. To investigate this behavior, the proton spectra of **1a** were recorded in the presence of increased amounts of $NC_5H_4CF_3$-4. As shown in Supporting Information, Figure S1, upon addition of 2 equiv of $NC_5H_4CF_3$-4, the pattern observed is identical to that obtained with crystals of complex **4**. Upon progressive addition of ligand, the resonances of **1a** gradually decrease, whereas those of complex **4** increase, and a large excess of pyridine (6 equiv) is required to completely move the equilibrium toward

complex **4**. The presence of only one set of pyridine protons (δ 8.87 $H^{2,6}$; 7.42 $H^{3,5}$), very close to those of free $NC_5H_4CF_3$-4 (δ 8.81 $H^{2,6}$; 7.51 $H^{3,5}$), supports its involvement in a fast additional exchange with complex **4**. The pyrazole derivative **5** exhibits (CD_2Cl_2), in addition to the aromatic tolyl protons, two characteristic resonances at δ 11.97 (br) and at 6.27 ppm (pt, $J = 2.4$ Hz) due to the H^1 and H^4 protons of the pyrazole, but only a broad signal ($\sim$ 7.34 ppm) for H^3 and H^5, indicating that they are also involved in a dynamic process. Upon cooling, coalescence is observed at about 293 K ($\Delta G_{293}^{\ddagger} \sim 58.43$ KJ·mol^{-1}) and, finally, the resonance split into two discrete signals (δ 7.50 and 7.17 ppm). Addition of a slight excess of pzH to this solution at room temperature (r.t.) only causes a significant sharpening of the $H^{3,5}$ resonance and a slight upfield shift for H^1 (δ 11.78 ppm), thus suggesting that a fast dissociative ligand process could be responsible for the observed average of H^3 and H^5 protons in this complex. The ^{195}Pt NMR spectrum of a $CDCl_3$ solution containing **4** and $NC_5H_4CF_3$-4 (1:4 molar ratio) could be also recorded (Figure 1), showing the presence of a singlet at -3761 ppm with both ^{111}Cd ($^1J(^{195}Pt-^{111}Cd) = 1855$ Hz) and ^{113}Cd ($^1J(^{195}Pt-^{113}Cd) = 1941$ Hz) satellites. The observed relative ratio 1:3:1 matches that expected for a tetranuclear Pt_2Cd_2 aggregate, ruling out the formation of binuclear Pt−Cd units (expected ratio 1:4:1) in the presence of excess of pyridine. We are not aware of previously reported one bond ^{195}Pt-^{111,113}Cd coupling constants.[55−57] In **4**, both the remarkable downfield of the platinum resonance in relation to the anionic precursor $(NBu_4)_2$-$[Pt(C{\equiv}CTol)_4]$ (δ −4187 ppm) and the high value of the Pt−Cd coupling constants are indicative of a relatively strong Pt→Cd dative bond.

X-ray Diffraction Studies. Perspective views of the molecular structures of tolylacetylide derivatives **2a**, **4** and **5** are represented in Figures 2, Supporting Information, Figure S2, and Figure 3, respectively, whereas those of the *m*-methoxyphenylacetylide complexes **2c** and the solvate **1c(dmso)$_2$** are shown in Figures 4 and 5. Selected bond lengths and angles are listed in Table 2. As can be seen, the molecules can be visualized as 2:2 adducts giving rise to final rhomboidal Pt_2Cd_2 cores, which are very *unsymmetrical* in the tolyl complexes (**2a**, **4**, **5**) and *symmetrical* in the *m*-methoxy derivatives **2c** and **1c-(dmso)$_2$**. One of the most striking features is that, in spite of the relatively hard nature of the acidic Cd^{II} ion and the presence of excess of ligand, it only forms one Cd−N-(imine) bond (2.239(3) Å **2a**; 2.245(4) **2c**; 2.277(3) **4**; 2.221(4) **5**). Similarly, in the solvate **1c(dmso)$_2$** the Cd is bonded to the oxygen atom of one dimethylsulfoxide molecule with a typical[58] bond distance of 2.224(6) Å. Curiously, in the tolylacetylide aggregates **2a**, **4**, and **5**, the Cd center of the resulting formed dicationic unit CdL^{2+}

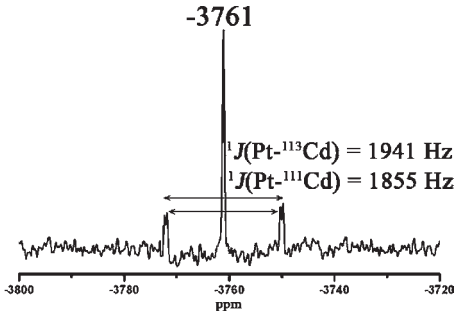

Figure 1. ^{195}Pt{^{1}H}NMR spectra of **4** + $NC_5H_4CF_3$-4 (6 equiv) in CD_2Cl_2 at 298 K.

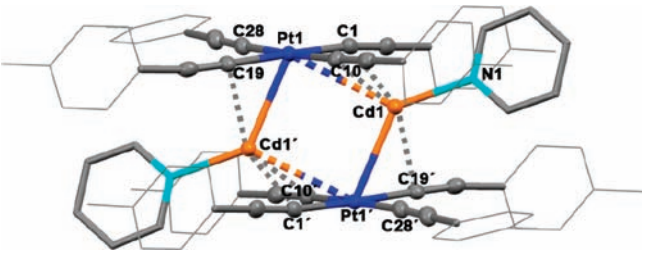

Figure 2. Molecular structure of $[Pt(C{\equiv}CTol)_4Cd(py)]_2$ **2a**. Only atoms of the central core ($Pt_2Cd_2(C{\equiv}C)_8$) are drawn as ellipsoids at the 50% probability level and hydrogen atoms omitted for clarity.

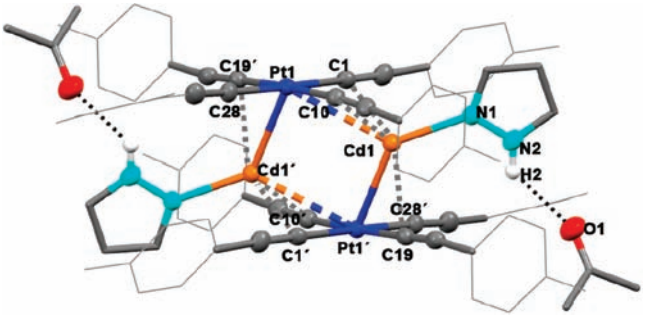

Figure 3. Molecular structure of $[Pt(C{\equiv}CTol)_4Cd(pzH)]_2 \cdot 2$acetone **5**·2acetone. Only atoms of the central core ($Pt_2Cd_2(C{\equiv}C)_8$) and nitrogens of the pyrazole ligand are drawn as ellipsoids at the 50% probability level, while hydrogen except H2, which is involved in H···O(acetone) contacts, are omitted.

forms a very short Pt→Cd donor−acceptor bond with the corresponding tetraalkynyl platinate. In fact, the Pt-(1′)−Cd(1) bond length (2.6999(3) Å **2a**; 2.7460(3) Å **4**; 2.6952(4) Å **5**) is shorter than the sum of the covalent radii (1.36 (Pt) + 1.44 (Cd) = 2.8 Å)[59] and lies in lower range of reported $Pt^{II}-Cd^{II}$ bond distances, being shorter to that found in [*cis*-$Pt(C_6F_5)_2(C{\equiv}CPh)_2Cd(cyclen)$] (2.764(1) Å)[39] and close to the shortest one reported to date by Ito et al.[55] in the cation $[(Phpy)_2PtCd(cyclen)]^{2+}$ (2.6389-(8) Å, Phpy = 2-phenylpyridinate). Although this fact points to the presence of a significant donation of the electron density from the d_{z^2}(Pt) orbital to the Cd^{II} cation, the Pt−Cd vector displaces from the normal to the platinate fragment (27.96° **2a**; 32.01° **4**; 26.94° **5**) toward one of the platinum-alkynyl units (Pt−C19−C20), also allowing a close Cd−$C^{\alpha'}$ contact (Cd−C19′ 2.491(4) Å **2a**;

(55) Yamaguchi, T.; Yamazaki, F.; Ito, T. *J. Am. Chem. Soc.* **1999**, *121*, 7405.
(56) Chen, W.; Liu, F.; Nishioka, T.; Matsumoto, K. *Eur. J. Inorg. Chem.* **2003**, 4234.
(57) Femoni, C.; Kaswalder, F.; Iapalucci, M. C.; Longoni, G.; Zachini, S. *Chem. Commun.* **2006**, 2135.
(58) (a) Marques, L. L.; de Oliveira, G. M.; Lang, E. S. *Z. Anorg. Allg. Chem.* **2006**, *632*, 2310. (b) Reddy, H. K.; Zhang, Ch.; Shlemper, E. O.; Schrauzer, G. N. *Inorg. Chem.* **1992**, *31*, 1673. (c) Halasz, I.; Horvat, M.; Biljan, T.; Mestrovic, E. *J. Chem. Cryst.* **2008**, *38*, 793. (d) Defazio, S.; Cini, R. *Polyhedron* **2003**, *22*, 1355.
(59) Cordero, B.; Gómez, V.; Platero-Prats, A. E.; Revés, M.; Echeverria, J.; Cremades, E.; Barragán, F.; Alvarez, S. *Dalton Trans.* **2008**, 2832.

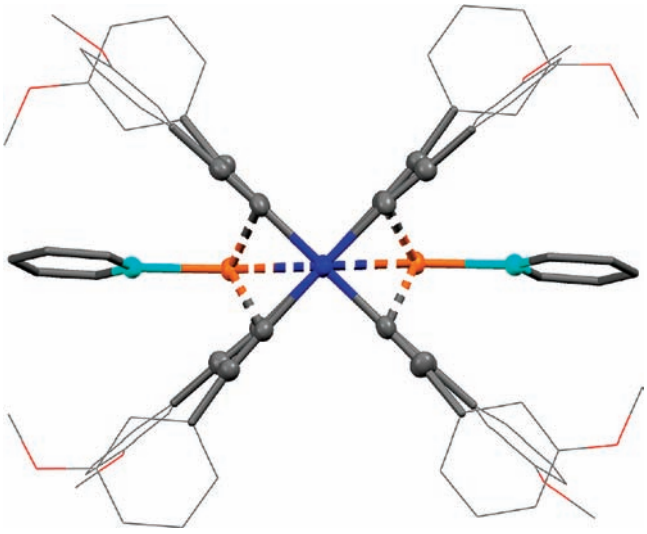

Figure 4. Zenith view of the molecular structure of $[Pt(C{\equiv}CC_6H_4OMe\text{-}3)_4Cd(py)]_2$ **2c** (50% probability ellipsoids). Aryl and pyridil atoms are simplified and hydrogen atoms are omitted for clarity.

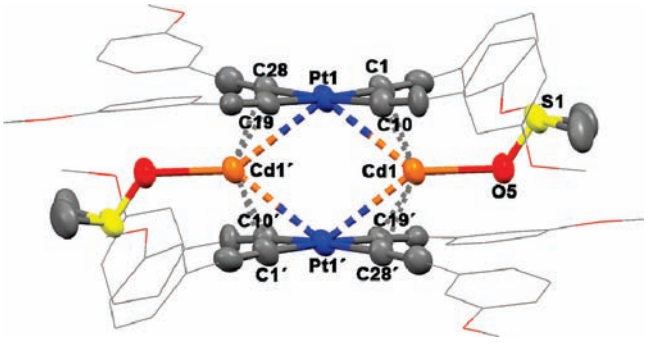

Figure 5. Molecular structure of $[Pt(C{\equiv}CC_6H_4OMe\text{-}3)_4Cd(dmso)]_2$ **1c(dmso)$_2$**. Only atoms of the central core ($Pt_2Cd_2(C{\equiv}C)_8$) and dmso are drawn as ellipsoids at the 50% probability level, and hydrogen atoms are omitted for clarity.

2.474(4) Å **4**; Cd−C19 2.495(5) Å **5**). The resulting neutral $\{Pt(C{\equiv}CR)_4CdL\}$ unit dimerizes by rather unsymmetrical η^2 interactions of the Cd^{II} with two mutually *cis* alkynyl fragments of the other unit, thus completing a distorted tetrahedral coordination around the Cd^{II} (See Supporting Information, Figure S2c for **4**). The observed Cd alkynyl interactions take place mainly with the C^{α} carbon atoms, with Cd−C^{α} distances in the range 2.409(4) to 2.450(4) Å. The Cd−C^{β} separations (2.644(4)−2.736(4) Å) are remarkably longer (0.22−0.32 Å) and only close to the sum of the van der Waals radii (2.7 Å) of C^{sp} (1.78 Å)[60] and the ionic radii of Cd^{II} (C.N. 4, 0.92 Å),[61] suggesting that the interaction with these atoms is very weak. Notwithstanding, to accommodate these weak Cd···C^{β} bonding interactions the platinate units displaced each other (ca. 1.33 Å **2a**; 1.85 Å **4**; 1.97 Å **5**), retaining an eclipsed disposition in **2a** and **5** or with a slight twisting (∼ 14°) in complex **4** (see Supporting Information, Figure S2). As a consequence of this relative orientation, the interaction of the Cd center with the platinum of the second platinate fragment is remarkably weaker (Pt(1)−Cd(1) 3.1186(3) Å **2a**; 3.0872(3) Å **4**; 3.1290(4) **5**), though still below the van der Waals limit (3.33 Å).[61] The resulting unsymmetrical rhomboidal metallic Pt_2Cd_2 array is planar in **2a** and **5** and slightly distorted in **4** (torsion angle 10.58°), with relatively long Pt···Pt (4.2525(2) Å **2a**; 4.0360(2) Å **4**; 4.3017(3) Å **5**) and Cd···Cd (3.9934(4) Å **2a**; 4.1948(4) Å **4**; 3.9503(6) Å **5**) separations. Curiously, in **2a** and **5** the corresponding pyridine and pyrazole planes are nearly contained in the metallic plane (small dihedral angles of 18.56° **2a** and 18.64° **5**). In complex **4**, probably because of the low basicity of the $NC_5H_4CF_3$-4, the pyridine plane is twisted 38.35° and the Cd−N vector is also slightly tilted (∼15°) in relation to the plane of the N-donor ligand (see Figure 2a), suggesting a misdirected interaction. As far as the bonding mode of the alkynyl ligands is concerned, it is noteworthy that, in agreement with the IR spectra, there are two ligands (C(28)−C(29)-Tol) that remain as terminal groups (one from each platinate unit), two acting as μ-κ^2C^{α} bridging ligands, and the remaining four that exhibit a rather unsymmetrical μ-κ^2C^{α}:η^2 bridging mode. Despite this dissimilarity no clear correlation can be found between the bonding mode and their structural details (see Table 2). The pyrazole derivative **5** crystallizes in the $P\bar{1}$ space group with one molecule of acetone in the unsymmetrical unit, whose oxygen atom (O1) is involved in intermolecular hydrogen bonds with the N−H hydrogen atom of the corresponding pyrazole groups (Figure 3). The H(2)···O(1) and N(2)···O(1) distances (2.198 and 2.861 Å respectively) and the N(2)−H(2)−O(1) angle (133.82°) are within the usual range for this type of contacts.[62−66]

The structures of the *m*-metoxyalkynyl derivatives **2c** and **1c(dmso)$_2$** (Figures 4 and 5, respectively) display a symmetrical framework in which the two tetraalkynyl platinates are eclipsed and both cationic cadmium units symmetrically bisect the alkynyl entities, being bonded to four Pt−C^{α} bonds (two associated with each platinum unit). As a consequence, in both derivatives the alkynyl ligands display a μ-κ^2C^{α} bonding mode and the Cd^{II} ion is in an approximately square pyramidal geometry, with the midpoint of the four Pt−C^{α} bonds occupying the basal plane, and the pyridine (**2c**) or the dmso (**1c(dmso)$_2$**) at the apex. Probably because of the higher coordination number (C.N. = 5), the Cd−C^{α} distances (range 2.471(5)−2.551(5) Å **2c**; 2.470(10)−2.508(10) Å **1c(dmso)$_2$**) are slightly longer to those found for the μ-κ^2C^{α} and μ-κ^2C^{α}:η^2 bridging ligands in the tolyl-acetylide derivatives (2.409(4)−2.495(5) Å). In the final rhomboidal planar $Pt_2Cd_2E_2$ (E = N, O) cores, the four Pt→Cd bonds are now nearly symmetrical (Pt−Cd 2.8001(4), 2.8505(4) Å **2c**; 2.9052(8), 2.9114(8) Å **1c(dmso)$_2$**). The value of the mean Pt−Cd separation in the pyridine complex **2c** (∼2.825 Å) is only somewhat shorter than the corresponding average

(60) Szafert, S.; Gladysz, J. A. *Chem. Rev.* **2003**, *103*, 4175.
(61) Winter, M. *The Periodic Table on the W.W.W.*; The University of Shefield and Web Elements Ltd.: U. K., 2008;www.webelements.com.
(62) Jeffrey, G. A. *An introduction to Hydrogen Bonding*; Oxford University Press: New York, 1997.
(63) Lyssenko, K. A.; Antipin, M. Y. *Russ. Chem. Bull., Int. Ed.* **2006**, *55*, 1.
(64) Knope, K. E.; Cahill, C. L. *Inorg. Chem.* **2009**, *48*, 6845.
(65) Xie, J.; Abrahams, B. F.; Wedd, A. G. *Chem. Commun.* **2008**, 576.
(66) Reddy, L. S.; Chandrau, S. K.; George, S.; Babu, N. J.; Naugia, A. *Cryst. Growth Des.* **2007**, *7*, 2675.

Table 2. Selected Bond Lengths [Å] and Angles [deg] for **2a**·2CH_2Cl_2, **4**·CH_2Cl_2, **5**·2acetone, **2c**·CH_2Cl_2, and **1c(dmso)$_2$**·2CH_2Cl_2

	2a·2CH_2Cl_2	**4**·CH_2Cl_2	**5**·2acetone	**1c(dmso)$_2$**·2CH_2Cl_2	**2c**·CH_2Cl_2
Pt(1)−Cd(1)	3.1186(3)	3.0872(3)	3.1290(4)	2.9052(8)	2.8001(4)
Pt(1′)−Cd(1)	2.6999(3)	2.7460(3)	2.6952(4)	2.9114(8)	2.8505(4)
Pt−C^{α}	2.005(3)−2.028(5)	2.001(4)−2.028(4)	1.993(5)−2.026(5)	2.007(10)−2.027(11)	2.009(4)−2.017(5)
Cd−C^{α}	2.435(4), 2.450(4)	2.409(4), 2.417(3)	2.424(5), 2.429(5)	2.470(10)−2.508(10)	2.471(5)−2.551(5)
Cd−C^{β}	2.669(4), 2.718(4)	2.644(4), 2.736(4)	2.644(5), 2.701(6)		
Cd−$C^{\alpha'}$	2.491(4)	2.474(4)	2.495(5)		
C^{α}−C^{β}	1.194(6)−1.228(5)	1.199(5)−1.209(5)	1.204(8)−1.215(8)	1.187(13)−1.207(13)	1.202(7)−1.213(7)
Cd(1)−N(1)	2.239(3)	2.277(3)	2.221(4)		2.245(4)
Cd(1)−O(5)				2.224(6)	
Cd(1)−Pt(1)−Cd(1′)	86.362(8)	91.772(9)	85.068(11)	102.27(2)	97.261(10)
Pt(1)−Cd(1)−Pt(1′)	93.638(8)	87.356(8)	94.933(11)	77.73(2)	82.740(10)
Pt−C^{α}−C^{β}	173.7(3)−177.1(4)	172.0(3)−175.2(3)	174.8(5)−178.2(5)	173.6(9)−175.4(9)	172.5(5)−178.8(4)
C^{α}−C^{β}−C^{γ}	172.7(4)−178.0(4)	171.2(4)−177.5(5)	172.3(6)−177.9(6)	173.4(12)−175.6(11)	171.0(5)−176.7(5)

values between the shortest and the longest Pt−Cd distances found in the unsymmetrical tolyl-derivatives (averages 2.9092 Å **2a**; 2.9166 Å **4**; 2.9121 Å **5**), suggesting that stabilization of these clusters involves a synergistic combination of Pt···Cd, Cd···alkynyl, and Cd−N bonding interactions. It should be pointed out that in **2c** and **1c(dmso)$_2$**, the presence of OMe substituents favors the existence of weak *intermolecular* non-covalent interactions, which lead to the generation of a complex supramolecular network (see Supporting Information, Figure S3 as illustration for **2c**) and, probably, are also playing a significant role in the stabilization of the final symmetrical Pt_2Cd_2 cores with a five coordination environment around the Cd^{II}. Although it is less obvious why similar symmetrical aggregates are not favored in the tolyl derivatives, it is clear that the preferred formation of a very short Pt→Cd bond in these latter (**2a**, **4**, and **5**) seems to be responsible for the absence of an interaction of the Cd^{II} with one of the alkynyl ligands, resulting in a final lower tetrahedral coordination.

Photophysical Characterization

Absorption Spectroscopy. The absorption data for all the complexes are summarized in Supporting Information, Table S1. In the solid state, the diffuse-reflectance of the yellow tetranuclear aggregates are characterized by a distinctive low energy feature in the range of 370 for **2c** to 385 nm for **2b** with a long tail to ~475 nm, which is absent in the white solvent-free **1′a**−**c** derivatives. By way of illustration, the spectra of the free **1′c** and solvate **1c(dmso)$_2$** and the pyridine adducts **2a**−**c** are given in Supporting Information, Figures S4 and S5, respectively.

As mentioned above, the solvates **1a,b(acetone)$_2$** $[Pt(C{\equiv}CR)_4Cd(acetone)]_2$, are only soluble in chlorinate solvents, in which they are unstable evolving to solvent-free insoluble derivatives **1′a**−**c**. The spectra of *freshly* prepared CH_2Cl_2 solutions of both complexes (see Supporting Information, Figure S6 for **1b(acetone)$_2$**) show several high energy features (200−266 nm, see Supporting Information, Table S1) due to intraligand transitions and a low energy absorption (316 nm **1a(acetone)$_2$**; 319 nm **1b(acetone)$_2$**), which appear remarkably blue-shifted in relation to the lowest $^1\pi\pi$ IL/dπ(Pt)→π^*(C≡CR) MLCT manifold in the corresponding precursors $[Pt(C{\equiv}CR)_4]^{2-}$ (CH_2Cl_2; 335, 345*sh* R = Tol; 344 R = C_6H_4OMe-4). Similar hypsochromic shifts have been previously observed in tweezer-like heterometallic Pt−Cd complexes and have been attributed to the existence of a lesser electronic dπ(Pt)/C≡C interaction caused by the *in-plane* η^2-Cd complexation, which probably lowers the energy of the alkynyl based highest occupied molecular orbital (HOMO).[29] The shift to higher energies observed for **1a,b(acetone)$_2$** in the low energy band suggests that, in CH_2Cl_2 solution, the acetone molecules are likely lost and the Cd^{II} centers probably move toward an *in-plane* η^2-coordination with the alkynyl ligands. In accordance with this suggestion, the progressive addition of acetone to the CH_2Cl_2 solution causes the growth of a new low energy band (372 nm, **1a(acetone)$_2$**; 377 nm, **1b(acetone)$_2$**; see Supporting Information, Figure S6 for **1b(acetone)$_2$**) similar to those observed for the tetranuclear aggregates **2**−**5** (vide infra), thus suggesting the coordination of the acetone molecules to Cd, with the concomitant formation of the solvate $[Pt(C{\equiv}CR)_4Cd(acetone)]_2$ species in solution to some extent. Similarly, only in the presence of an excess of dmso (mixture CH_2Cl_2:dmso 9:1) does the spectrum of **1c(dmso)$_2$** show two low energy bands (348 and 371 nm), and a similar pattern to that observed for the pyridine clusters (345, 377 nm **2a**, 348, 375 nm **2c** and 348, 376 nm **3**), which seems to be characteristic of the tetranuclear cluster entities $[Pt_2(C{\equiv}CR)_8Cd_2L_2]$ (Figure 6). Along the same lines, the existence of a remarkable dissociation of the $NC_5H_4CF_3$-4 ligand for **4**, was also confirmed by UV−vis spectroscopy. By way of illustration, Figure 7 shows the spectra of the precursor **1a(acetone)$_2$** and the microcrystalline solid **4**, together with the changes observed upon addition of $NC_5H_4CF_3$-4.

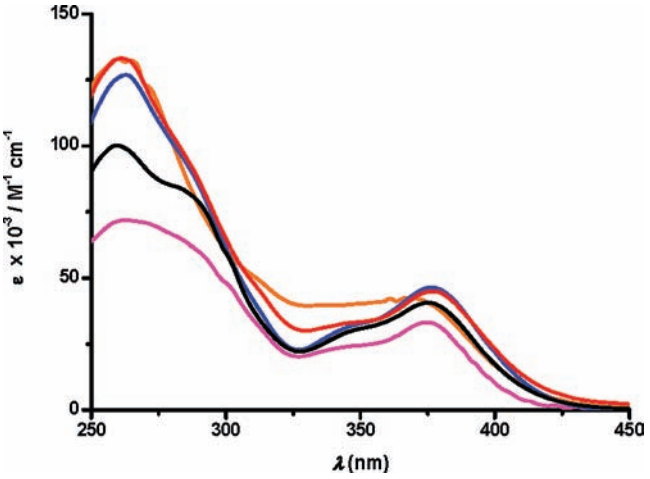

Figure 6. Absorption spectra of **1c(dmso)$_2$** in a mixture CH_2Cl_2:dmso (9:1) (pink) and **2a** (red), **2c** (black), **3** (blue), and **5** (orange) in CH_2Cl_2 (5×10^{-5} M).

The band at ~316 nm, which resembles the ^{1}IL/MLCT band of the precursor, is progressively depleted, while the band at 376 nm due to **4** grows and a shoulder at 348 nm, typical of the tetranuclear aggregates, is also clearly seen when more than 10 equiv of $NC_5H_4CF_3$-4 are added. The presence of a clear isosbestic point indicates that a simple equilibrium between **1a** and **4** is involved.

The two distinctive low energy absorptions exhibit a small dependence on the alkynyl substituents and the coligands at cadmium. Thus, a slight blue shift is observed from **2a** (Tol, py) to **2c** (C_6H_4OMe-3, py) and, in the tolyl derivatives, the energy follows the order **5** (367 nm) > **1a(acetone)$_2$** (372 nm) > **2a** (377 nm) ~ **3** (377 nm) ~ **4** (376 nm). Following previous assignments,[24,30,34,38] these low energy absorptions are primarily attributed to an admixture of singlet Pt/π(C≡CR)→π*(C≡CR) (MLCT) and platinum-ligand to cadmium charge transfer Pt-(C≡CR)→Cd. Alternatively, we denoted the transition as ^{1}MLM′CT (M = Pt, M′ = Cd) with intraligand ($^1\pi\pi$ C≡CR) character. In the observed trend the influence of the nature of the coligands at Cd is not so clear. However, the coordination of pyridine ligands causes a slight red shift in the absorption maxima, most likely because of an increased character from platina-alkynyl to pyridine charge transfer character MLL′CT, as suggested by TD-DFT calculations.

Emission Spectroscopy. Probably because of the rigidity of the tetranuclear rhomboidal systems, aggregates **1a,b(acetone)$_2$**, **1c(dmso)$_2$**, **2**−**5** are strongly emissive in the solid state (298, 77 K), with high quantum yields in the 4.5−36.3% range for the nitrogen coordinated derivatives **2**−**5** (Table 3). The latter also exhibit moderate luminescence in CH_2Cl_2 solution at 298 K. The calculated emission lifetimes fit to monoexponential decays in the range of microseconds, revealing their triplet state parentage. Figure 8 shows the emission spectra of the yellow solvate complexes in the solid state at 298 and 77 K. They exhibit a bright greenish luminescence (488 nm **1a(acetone)$_2$**, 515 nm **1b(acetone)$_2$**, 500 nm **1c(dmso)$_2$**), which is blue-shifted and slightly structured at 77 K (λ_{max} 484 nm **1a(acetone)$_2$**, 489 nm **1b(acetone)$_2$**, 492 nm **1c-(dmso)$_2$**), pointing to the involvement of the alkynyl ligands in the excited state. The emission occurs at lower energies compared to that of the anionic precursors,[40]

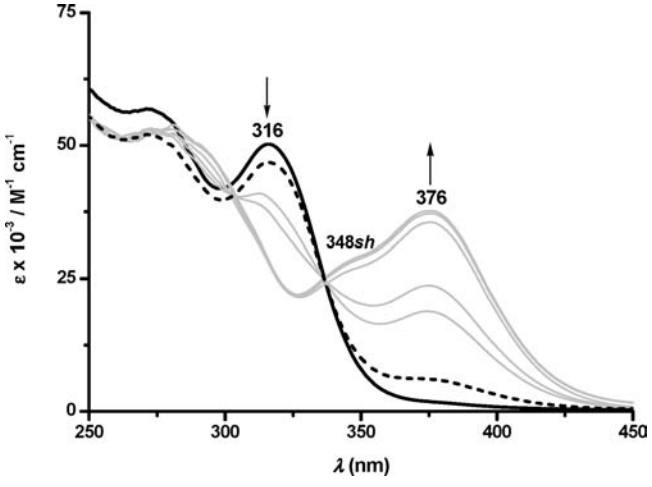

Figure 7. Absorption spectra of freshly prepared solution of **1a-(acetone)$_2$** (black) and **4** (dashed) in CH_2Cl_2 (5×10^{-5} M). In light gray, successive additions of 2, 6, 8, 18, and 38 equiv of $NC_5H_4CF_3$-4 to the solution of **4**, showing the growth of the band at 376 nm and the appearance of a shoulder at 348 nm, together with the decrease of the band at 316 nm upon the addition of ligand.

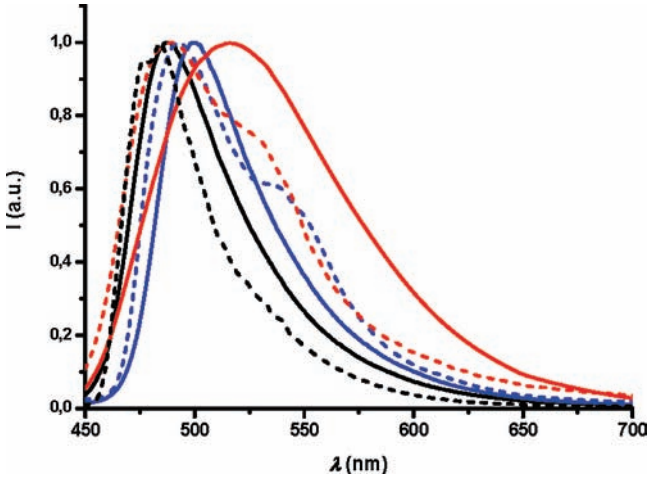

Figure 8. Normalized emission spectra for solid samples of **1a(acetone)$_2$** (black), **1b(acetone)$_2$** (red), and **1c(dmso)$_2$** (blue) at 298 (solid line) and 77 K (dashed).

Table 3. Emission Data for Complexes **1**−**5**

	solid state λ^{em}_{max}/nm [τ/μs] {ϕ/%}		
complex	298 K	77 K	CH_2Cl_2 5×10^{-5} M (298 K) λ^{em}_{max}/nm [τ/μs]
1′a	a	514 [8.8]	b
1′b	a	525 [7.8]	b
1′c	a	468_{max}, 507*sh*	b
1a(acetone)$_2$	488 [13.5]	484, 512*sh* [14.3]	
1a	510 [12.7]	501 [13.0]	
1b(acetone)$_2$	515	489, 509*sh*	
1b	560 [10.7]	540 [11.4]	
1c(dmso)$_2$	500	492_{max}, 532*sh*	
2a	490 [8.0] {4.5}	479 [9.3]	533
2b	520 [7.2] {15.2}	500 [9.2]	b
2c	492 [14.5] {6.9}	469, 512*sh* [9.6]	528 [11.0]
3	488 [11.7] {10.5}	477, 512*sh* [17.6]	532
4	505 [14.1] {13.3}	506 [15.1]	546[c]
5	545 [10.2] {36.3}[d]	530 [8.7][d]	567 [9.1]

[a] Not emissive at 298 K. [b] Not soluble. [c] Measured with excess of $NC_5H_4CF_3$-4 (1:10). [d] Measured over crystals containing acetone molecules (**5**·2acetone).

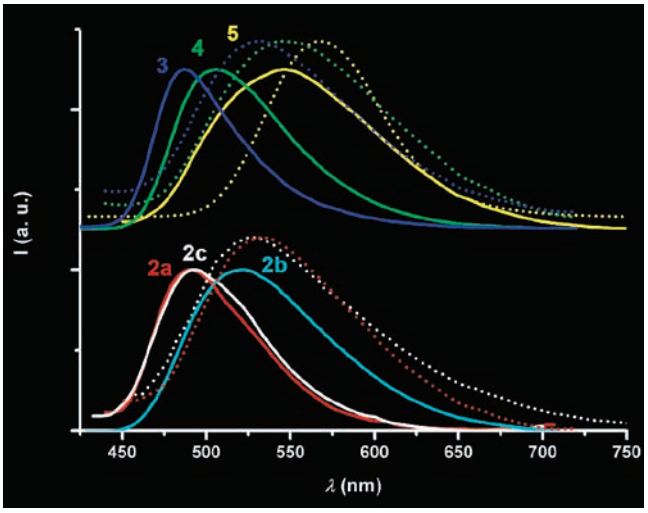

Figure 9. Emission spectra at room temperature of complexes **2a** (red), **2b** (light blue), **2c** (white), **3** (blue), **4** (green), and **5** (yellow) in the solid state (solid lines) and 5×10^{-5} M CH_2Cl_2 solution (dotted lines).

and decreases (Tol > C_6H_4OMe-3 > C_6H_4OMe-4) with the electron donating ability of the alkynyl groups, indicating that they must be involved in the lowest excited state. We assign the emission in these solvates as platinum-alkynyl to cadmium charge transfer with intraligand character ^{3}MLM′CT/^{3}ILC≡CR (Pt(d)/π(C≡CR)→Pt-(P_z)Cd(s)/π*(C≡CR)), as supported by the DFT studies (vide infra). Interestingly, the acetone molecules are removed from the solvate derivatives **1a,b(acetone)$_2$** upon prolonged vacuum at about 60−70 °C (48 h, **1a(acetone)$_2$**; 34 h, **1b(acetone)$_2$**), affording final ochre-orange solids (**1a**,**b**), which are weakly emissive (photographic images are shown in Supporting Information, Figure S7), displaying broader red-shifted emission bands centered at about 510 nm (**1a**) and 560 nm (**1b**), respectively (see Supporting Information, Figure S8 for **1a**). The process is reversible for several cycles (at least 4), and the initial yellow colors and green luminescence are recovered upon exposure of the orange solids to a drop of acetone. We think that the loss of acetone probably takes place with retention of the sandwich type structure. The change in color and the observed bathochromic shift in the emissions could be ascribed to the existence of stronger out of plane alkynyl-η^2-cadmium bonding interactions in **1a**,**b** in relation to the solvates, which presumably lower the energy of the π*(C≡CAryl) fragments, reducing the transition gap. The white free solvent-insoluble materials **1′(a−c)** are, however, only weakly emissive at low temperature (see Table 3).

At room temperature microcrystalline solids **2**−**5** display (Figure 9, solid lines) structureless emission bands in the range of 488 to 545 nm. Despite the presence of very short Pt−Cd donor−acceptor bonds, in all cases the emission maxima are blue-shifted at 77 K (469−530 nm see Table 3), suggesting that these bonds are not the primary contributors to the emissive manifolds. Interestingly, the emission band of these complexes is significantly red-shifted in CH_2Cl_2 solution (Figure 9, dotted lines) from those in the solid state. This behavior, denoted as rigidochromism, has been previously observed in other heteropolynuclear Pt_2M_4 (M = Cu, Ag, Au) complexes,[38,67] being attributed to structural changes in the excited state, which are more favorable in solution than in the rigid lattice of the solid.[68] Curiously, with exception of the pyrazole derivative **5** (712 cm^{-1}), the extent of the red-shifts in solution is higher in the unsymmetrical tolylalkynyl derivatives (1646 **2a**, 1695 **3**, and 1487 cm^{-1} **4**) than in the symmetrical meta-methoxyalkynyl complex **2c** (1385 cm^{-1}). It is likely that the clusters in solution adopt a symmetrical Pt_2Cd_2 central core with a final square-planar pyramidal coordination around the Cd centers, which could be closer to that seen for **2c** in the solid state (C.N. = 5) than for the unsymmetrical tolyl derivatives (distorted tetrahedral C.N. = 4). It is noteworthy that the excitation spectra in solution resemble the corresponding absorption spectra, suggesting that the emission comes from the tetranuclear {Pt_2(C≡CR)$_8$$Cd_2$-$L_2$} aggregates (see Supporting Information, Figure S9 for complex **3**). As can be seen in Figure 9, the emission energy was found to change upon variation of both the alkynyl ligand and the N-donor ligand at cadmium. The latter has a prominent effect on the emission energy, following the same trend in the solid state (488 **3** > 490 **2a** > 505 **4** > 545 nm **5**) as in solution (532 **3** > 533 **2a** > 546 **4** > 567 nm **5**), which is in line with the electron-accepting ability of the N-imine ligand ($NC_5H_4CH_3$-4 < NC_5H_5 < $NC_5H_4CF_3$-4 < pzH). Furthermore, both at 298 and at 77 K the emission energy of **2b** (520 nm 298 K; 500 nm 77 K) is red-shifted in relation to **2c** (492 nm 298 K; 469 nm 77 K) and **2a** (490 nm 298 K; 479 nm 77 K). This fact reflects the role of the better electron delocalization between the C≡C and aryl in the *p*-methoxyphenylethyl fragment, which reduces the transition gap. Taking into account these trends and the salient features of the frontier orbitals (see below), which indicate the role of the pyridine ligands in the lowest unoccupied molecular orbitals LUMO and LUMO+1 for complexes **2a**, **2c**, and **4** and of the Pt_2Cd_2 metallic core in the pyrazole derivative **5**, we suggest that the emission comes from an excited state of large Pt(d)/π(C≡CR)→π*(imine) MLL′-CT character, mixed with Pt(d)π(C≡CR)→Pt_2Cd_2/π*-(C≡CR) (MLM′CT) contribution, this latter being particularly remarkable in complex **5**. It should be noted that the observed trend coincides only roughly with the calculated triplet excitations from DFT calculations, and for complexes **4** and **5** this is even reversed (see Supporting Information, Table S2). This suggests that in these systems the calculated forbidden absorption is likely only a poor approximation to the emissive excited state. In addition, in the case of the pyrazole complex **5** the presence of the acidic N−H proton and its involvement in the dynamic process (vide supra) through a possible interaction with the alkynyl fragments could be responsible for the remarkable red shift (calculated 434 nm, experimental 538 nm). Upon cooling the CH_2Cl_2 solutions to 77 K, the emission bands shift remarkably to higher energies exhibiting somewhat structured profiles (see Supporting Information, Figure S10) with λ_{max} at 460 **2a**, ~ 450 (**3**, **4**) and 496 nm **5**. Although less structured, the emissions of **2a**, **3**, and **4** resemble those found

(67) Umakoshi, K.; Saito, K.; Arikawa, Y.; Onishi, M.; Ishizaka, S.; Kitamura, N.; Nakao, Y.; Sakaki, S. *Chem.—Eur. J.* **2009**, *15*, 4238.

(68) Ford, P. C.; Cariati, E.; Bourassa, J. *Chem. Rev.* **1999**, *99*, 3625.

Table 4. Molecular Orbital Composition in Terms of Ligands and Metals for Complexes **1c(dmso)$_2$**, **2a**, **2c**, **4**, and **5**

	1c(dmso)$_2$				**2a**				**2c**				**4**				**5**			
MO	Pt	Cd	C≡CR	dmso	Pt	Cd	C≡CR	py	Pt	Cd	C≡CR	py	Pt	Cd	C≡CR	py	Pt	Cd	C≡CR	pzH
LUMO+3	3	2	94	1	0	1	4	96	0	0	16	84	0	0	4	95	3	3	25	69
LUMO+2	5	11	82	3	29	13	54	3	25	10	60	5	27	13	58	2	0	1	9	90
LUMO+1	4	10	85	1	0	1	2	97	0	1	9	91	0	1	2	98	18	11	53	17
LUMO	22	11	67	0	0	1	2	97	0	1	9	91	0	1	2	98	29	13	58	1
HOMO	20	1	79	0	14	0	86	0	15	1	84	0	15	1	84	0	15	2	83	0
HOMO-1	21	1	78	0	15	2	83	0	10	2	88	0	14	1	85	0	13	0	86	0
HOMO-2	16	2	81	1	14	1	85	0	16	1	83	0	12	2	76	0	17	1	82	0
HOMO-3	18	2	80	1	14	2	83	0	14	2	84	0	19	2	78	1	18	3	79	0

in $(NBu_4)_2[Pt(C{\equiv}CTol)_4]$ (λ_{max} 447, 465, 475, 480 nm),[40] suggesting that in frozen CH_2Cl_2 their emissions could be tentatively ascribed to a $^3IL(\pi\pi^*)/^3MLCT$ manifold of the platinate fragments. The change of emission origin from the MLL′CT [Pt(d)/π(C≡CR)→π^*(pyridine)] excited state to a mixed $^3IL\pi\pi^*$(C≡CR)/^{3}MLCT manifold by lowering of the medium temperature indicates that these two excited states are likely close-lying in energy. However, for **5** the emission is broader and red-shifted in relation to $[Pt(C{\equiv}CTol)_4]^{2-}$, clearly showing the influence of the "Cd(pzH)" units.

Molecular Orbital Calculations. DFT calculations are currently used to establish electronic structures and spectral transitions. In this work, single point (DFT) and TD-DFT calculations were performed for **1c(dmso)$_2$**, **2a,c**, **4**, and **5**. Table 4 summarizes the orbital compositions for all five complexes in terms of ligands and metals. As can be seen, the calculations reveal some differences between the pyridine-cadmium coordinated aggregates (**2a,c**, **4**) and complexes **1c(dmso)$_2$** and **5**. The three pyridine complexes **2a,c** and **4** have similar frontier orbitals, those of **2a** are shown in Figure 10, and those of **2c** and **4** in Supporting Information, Figure S11. In these complexes, the last highest occupied molecular orbitals possess a strong alkynyl and platinum character. Thus, the HOMO and HOMO-1 derive from the combination of the Pt(II) dπ orbitals (∼ 15%) with two mutually *trans* π(C≡CAryl) (83−86%) alkynyl ligands on each platinate fragment, and the HOMO-2 and HOMO-3 are similar, but are built up from the other mutually *trans* alkynyl ligands. The LUMO and LUMO+1 are mainly composed of the π^* of the pyridine ligands (97% **2a**; 91% **2c**; 98% **4**) with a negligible contribution of metals (Cd ∼ 1%) and alkynyl fragments. However, the LUMO+2, which is ∼0.43 (**2a**), 0.34 (**2c**), and 0.79 eV (**4**) higher than the LUMO, has alkynyl (54−60%) and remarkable Pt_2Cd_2 metallic (Pt(p) 25−29%/Cd(s) 10−13%) character. As can be seen in Table 4 (see also Figure 10 and Supporting Information, Figure S11), for complexes **1c(dmso)$_2$** and **5**, the composition of the HOMOs (HOMO-3 to HOMO) is essentially similar to those for **2a,c** and **4**, being composed of platinum and alkynyl ligands. However, in these derivatives there is a major difference in the unoccupied orbitals, because the LUMO and LUMO+1 are now metal and alkynyl ligand based. Thus, for both **1c(dmso)$_2$** and **5** the LUMO is a cluster-localized Pt_2Cd_2 metallic orbital (Pt (22−29%), mainly p_z; Cd (11−13%) mainly s), which exhibits σ Cd−Cd bonding character with remarkable alkynyl contribution (67, 58%). In the LUMO+1 the contribution of cadmium in both complexes is similar to that of LUMO, while that of Pt(II) is lower.

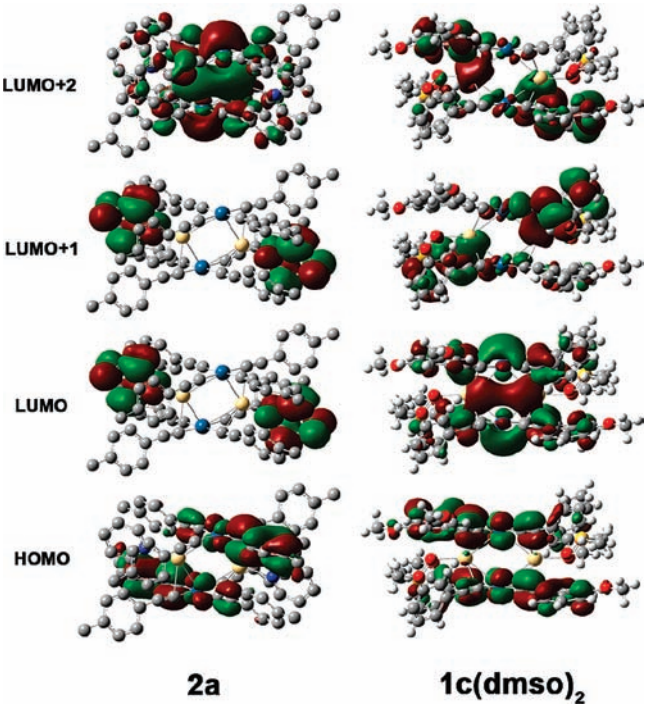

Figure 10. Frontier orbital plots for **2a** and **1c(dmso)$_2$** obtained by DFT.

The difference between **1c(dmso)$_2$** and **5** is observed in the following unoccupied orbitals. In **1c(dmso)$_2$** the LUMO+2 and LUMO+3 have preponderant alkynyl contribution, while in the pyrazole derivative **5** the LUMO+2 is composed of 90% of pzH, and the LUMO+3 contains contributions from pzH (69%) and C≡CTol (25%).

The nature of the absorption features were explored by TD-DFT calculations using the polarized continuum model in which the solvent is simulated as a continuum of uniform dielectric constant. Calculated transitions energies in CH_2Cl_2 solutions (first singlets) with strong oscillator strengths, which have a higher contribution to the absorption spectra, are summarized in Supporting Information, Table S2. For complex **1c(dmso)$_2$**, the lowest-energy absorptions (HOMO-*n* to LUMO) involve transitions from platinum-alkynyl orbitals based (PtC≡CR) to the LUMO, a (Pt_2Cd_2)/π^*C≡CR orbital, which can be assigned as MLM′CT (M = Pt, M′ = Cd) platinum-alkynyl-to-cadmium charge transfer. The calculated values (353, 346, 331 nm) can be related to experimental values seen in CH_2Cl_2 (371, 348*sh* nm) (Figure 6). A similar assignment can be made for complex **5**. In this complex, the three lowest computed absorptions are calculated at 380, 356, and 351 nm, resulting mainly from

HOMO→LUMO, HOMO-3→LUMO, and HOMO-1→LUMO+1, respectively. Experimentally, the lowest band is located at 367 nm, exhibiting a long tail spreading down to ~430 nm. In the pyridine derivatives the lowest energy absorptions calculated (348−369 nm **2a**; 345−370 nm **2c**; 329−395 nm **4**) correspond to the excitations from HOMO-*n* to LUMO, LUMO+1, and LUMO+2 (see Supporting Information, Table S2). Therefore, as the LUMO and LUMO+1 are π^* orbitals localized in the pyridine ligands and LUMO+2 is $Pt_2Cd_2/\pi^*C{\equiv}CR$ based in these aggregates, the two low energy absorptions can be assigned as admixture of $PtC{\equiv}CR\rightarrow\pi^*$(pyridine) (MLL′CT) and MLM′CT. This involves charge transfer from the platina-alkynyl fragments to the pyridine ligand, mainly in the lowest feature for **2a,c** (Figure 6), but also to the metallic core and $\pi^*C{\equiv}CR$ ($Pt_2Cd_2/\pi^*C{\equiv}CR$).

Conclusions

In summary, a series of sandwich-type tetranuclear yellow solvate complexes $[Pt(C{\equiv}CR)_4Cd(acetone)]_2$ **1a**,**b(acetone)$_2$** (Tol **a**, C_6H_4OMe-4 **b**) or $[Pt(C{\equiv}CC_6H_4OMe\text{-}3)_4Cd(dmso)]_2$ **1c(dmso)$_2$** or white polymeric free solvate $[Pt(C{\equiv}CR)_4Cd]_x$ **1′a**−**c** are generated from reaction between the anionic homoleptic substrates $[Pt(C{\equiv}CR)_4]^{2-}$ and Cd^{2+}. The formation of the white polymeric insoluble species, likely stabilized by η^2-alkynyl bonds, results from the weakness of the Cd···acetone bonding interactions. In fact, **1a**,**b(acetone)$_2$** are not stable in chlorinated solvents, evolving irreversibly to the final insoluble **1′a**,**b** species. However, in the solid state, the solvates **1a,b(acetone)$_2$**, which exhibit a bright green luminescence (488 **a**, 515 nm **b**), reversibly lost the acetone molecules affording ochre-orange solids with a very weak red-shifted emission (~510 **1a**, 560 **1b**). It has been found that addition of N-donors ligands results in the formation of stable **2**−**5** tetranuclear complexes, in which two dicationic CdL^{2+} units are stabilized by the synergistic combination of Pt···Cd and Cd···alkynyl bonding interactions. As revealed by X-ray crystallographic studies, the meta-methoxy-alkynyl derivatives (**1c(dmso)$_2$** and **2c**), which exhibit a different kind of secondary weak extended intermolecular interactions, form a planar symmetrical rhomboidal Pt^2Cd^2 framework (Pt···Cd ~ 2.85 Å) in which the Cd^{II} center adopt a final pyramidal geometry (C.N. = 5). By contrast, the tolylacetylide derivatives (**2**, **4**, and **5**) display planar unsymmetrical metallic frameworks with two short (~2.7 Å) and two weaker (~3.1 Å) bonding interactions, in which the Cd^{II} centers achieve a lower distorted four coordinated tetrahedral environment. As a consequence, these latter exhibit three different alkynyl ligation modes (μ-η^2, μ-κC^{α} and σ-C≡CR), while in **1c(dmso)$_2$** and **2c** all alkynyls adopt a μ-κC^{α} bonding mode. Probably because of the rigidity of these tetranuclear heterometallic systems (**2**−**5**) all clusters display bright solid state (Φ from 4,5 to 36.3%) and solution phosphorescence. As noted in the Introduction, it is now well established that the presence of $d^8\cdots d^{10}$ metallophilic interactions has a remarkable impact on the emission of heteropolynuclear complexes. In these systems, probably because of the presence of low-lying π^* orbitals on alkynyl and pyridine ligands, the contribution of the Pt···Cd bonds is less significant, and clearly these bonds are not the primarly contributors to the emissive manifolds. In the solid state and in fluid solution the emission maxima depend on the alkynyl substituent and the coligands. Both the experimental data and TD-DFT calculations suggest that excitation of these clusters moves electron density from both platina-alkynyl fragments toward low-lying orbitals, which have strong metallic/alkynyl ($Pt_2Cd_2/\pi^*C{\equiv}CR$) character in the case of the solvate and pyrazole (**5**) derivatives or a remarkable contribution of the π^* pyridine groups in the pyridine derivatives **2**−**4**. In the pyrazole derivative **5**, the possible interaction between the NH protons with the alkynyl fragments could be responsible for the lower HOMO−LUMO gap observed experimentally. All these properties may be useful in potential practical applications.

Acknowledgment. We thank the Spanish MICINN for financial support (Project CTQ2008-06669-C02-02). J.F. thanks the CAR (Colabora 09/15) and S.S. thanks the CSIC for a grant. We also thank CESGA for computer support.

Supporting Information Available: Diffuse reflectance and absorption data for complexes **1**−**5** in the solid state and solution, respectively (Table S1). Calculated transition energies in CH_2Cl_2 solutions for **1c(dmso)$_2$**, **2a**, **2c**, **4**, and **5** (Table S2). ^1H NMR of a $CDCl_3$ solution of **1a** upon progressive additions of $NC_5H_4CF_3$-4 (Figure S1). ORTEP views of complex **4** (Figure S2). Supramolecular details and views of the tridimensional organization of complex **2c** (Figure S3). Solid diffuse reflectance of complexes **1′c**, **1c(dmso)$_2$**, **2a**, **2b**, and **2c** (Figures S4 and S5). Absorption spectra of a freshly prepared solution of **1b(acetone)$_2$** in CH_2Cl_2 and in different mixtures of CH_2Cl_2:acetone (Figure S6). Photographic images under white and UV light of **1a(acetone)$_2$** and its reversible transformation into **1a** (Figure S7). Emission spectra of **1a(acetone)$_2$** and **1a** in the solid state at 298 K (Figure S8). Absorption and excitation spectra of a CH_2Cl_2 5×10^{-5} M solution of **3** (Figure S9). Emission spectra of CH_2Cl_2 5×10^{-5} M solutions of **2a**, **3**, **4**, and **5** at 77 K (Figure S10). Frontier orbital plots for **2c**, **4**, and **5** (Figure S11). Crystallographic data in CIF format. This material is available free of charge via the Internet at http://pubs.acs.org.